Electrical Properties of Dislocations within the Nitride Based Semiconductors Gallium Nitride and Indium Nitride

by

Erfan Baghani

B.Sc., Sharif University of Technology, 2005

M.Sc., Sharif University of Technology, 2007

A THESIS SUBMITTED IN PARTIAL FULFILLMENT OF

THE REQUIREMENTS FOR THE DEGREE OF

DOCTOR OF PHILOSOPHY

in

The College of Graduate Studies

(Applied Science)

THE UNIVERSITY OF BRITISH COLUMBIA

(Okanagan)

October 2012

© Erfan Baghani, 2012

Abstract

Dislocation lines affect the electrical and optical properties of semiconductors. In this research, the effect that the threading dislocation lines have on the free electron concentration and the electron mobility within gallium nitride and indium nitride is investigated. A formulation is developed for obtaining the screening space charge concentration and the corresponding electrostatic potential profile surrounding the dislocation lines. The resultant electrostatic potential profile has then been used to compute the associated electron mobility, limited by scattering from the charged dislocation lines. As part of this research, a Gibbs factor formalism is also developed that can readily obtain the occupation statistics of the defect sites associated with the threading dislocation lines.

Preface

This thesis, entitled "Electrical Properties of Dislocations within the Nitride Based Semiconductors Gallium Nitride and Indium Nitride," presents the research performed by Erfan Baghani. This research was supervised by Dr. Stephen K. O'Leary of The University of British Columbia.

A portion of the contents of Chapters 2 and 3 is published (Baghani and O'Leary 2011) "Electron mobility limited by scattering from screened positively charged dislocation lines within indium nitride", *Appl. Phys. Lett.*, vol. 99, pp. 262106-1-3. These results were produced using an iterative procedure that was developed by the author of this thesis.

A version of the contents of Section 4.5 is published (Baghani and O'Leary 2011) "Occupation statistics of dislocations within uncompensated n-type wurtzite gallium nitride", *J. Appl. Phys.*, vol. 109, pp. 113706-1-6. This section includes the original work of the thesis author, on the development and application of a Gibbs factor formalism to the problem of determining the occupation statistics of the dislocation lines with an assumed dangling bond dislocation core structure.

A version of the results presented in Section 4.6 is published (Baghani and O'Leary 2011) "Occupation statistics of the $V_{Ga} - O_N$ dislocations within n-type gallium nitride", *J. Appl. Phys.*, vol. 110, pp. 033509-1-6. This section

includes the original work of the thesis author, on the application of a Gibbs factor formalism to the problem of determining the occupation statistics of the dislocation lines with an assumed $V_{Ga} - O_N$ dislocation core structure.

Contents

List of Tables

List of Figures

Acknowledgements

I would like to express my sincere thanks to my supervisor, Dr. Stephen O'Leary, who gave me the chance for being involved in this interesting and challenging research project, and spent hundreds of hours of his time discussing various aspects of my work. His warm attitude has always inspired and encouraged me through these years. I would also like to thank my committee members, Dr. Jonathan Holzman and Dr. Kenneth Chau, for the fruitful discussions and helpful hints, and for providing me with support along the way.

The financial support for my study was provided by a research grant from the Natural Sciences and Engineering Research Council of Canada (NSERC) and from the College of Graduate Studies of the Okanagan campus of The University of British Columbia.

Chapter 1

Introduction

1.1 Motivation for the study of the nitride based semiconductors

The III-V nitride semiconductors, gallium nitride (GaN), indium nitride (InN), and aluminum nitride (AlN), possess a number of interesting material properties that make them suitable for a wide variety of important electronic and optoelectronic device applications [1, 2, 3, 4]. In terms of electronics, the wide energy gap of GaN, 3.39 eV at room temperature, makes it possible to use this material in high-frequency and/or high-power electron device applications [5, 6]. In terms of optoelectronics, the direct nature of the energy

gap associated with these materials, and the fact that ternary and quaternary alloys of these materials can be epitaxially grown, allows for their use in optoelectronic device applications, ranging from the near-infrared to the ultraviolet [7]. While initial attempts to fabricate electron devices with these materials were hindered by growth difficulties, many of these problems have now been solved. As a consequence, functional electron devices have been fabricated using GaN, InN, and AlN, and alloys of these materials [7, 8, 9]. This has generated considerable interest in the III-V nitride semiconductors.

Pioneering investigations into GaN were performed in the early 1930s by Johnson *et al.* [10]. The GaN samples considered in these early investigations were prepared through the interaction of ammonia gas with metallic gallium at elevated temperatures. Later, reactive sputtering was used in order to grow thin films of this material. Workers, such as Hovel and Cuomo [11], Malyutin *et al.* [12], Vesely *et al.* [13], Hariu *et al.* [14], Lakshmi *et al.* [15], Matsushita *et al.* [16], and Kubota *et al.* [17], employed this approach in order to understand the physical properties of this material. Unfortunately, the materials produced were polycrystalline in nature and not of the high quality crystalline form required for the electron device applications presently envisioned for this material.

A successful means of epitaxially growing high quality crystals of GaN was

found through the use of chemical vapor deposition (CVD). This approach to growing crystalline GaN was first employed by Maruska and Tietjen in 1969 [18]. In their approach, HCl vapor was allowed to react with metallic gallium, the resultant chemical species reacting with ammonia gas at the substrate. A number of variations on this approach have been developed through the years, including those by Pankove *et al.* [19], Crouch *et al.* [20] and Adonin *et al.* [21]. CVD remains a popular means whereby crystalline GaN may be fabricated.

Molecular beam epitaxy (MBE) may also be employed for the deposition of crystalline GaN. Initially, it was thought that MBE would allow for growth at lower temperatures than those required of CVD. In principle, this should allow for greater control over the growth process, thereby permitting the increased incorporation of nitrogen and reducing the unwanted high background electron concentration typically found in GaN. In addition, MBE was viewed as a promising technique for the growth of nitride-based heterostructures. Unfortunately, the promise that MBE offered failed to meet some of these lofty expectations, probably as a consequence of low reaction rates. Nevertheless, MBE remains a popular means of depositing customized devices fabricated with GaN.

Juza and Hahn [22] were the first researchers to synthesize InN. They

grew their samples using the same deposition procedure as that employed by Johnson *et al.* [10], i.e., through the interaction of ammonia gas with metallic indium at elevated temperatures. It was not until the 1960s, however, that research into InN was further pursued. Following the lead of GaN researchers, reactive sputtering was used in order to grow thin films of InN. Researchers, such as Pastrnak and Souckova [23], Hovel and Cuomo [11], and Tansley and Foley [24] used this technique in order to explore the properties of InN. Later, CVD and MBE were used in order to fabricate high quality samples of crystalline InN [23, 25, 26].

A major breakthrough occurred in 2002, stemming from the much improved quality of InN films grown through MBE. The bandgap of the resulting epitaxial films was found to be 0.64 eV [27]; previous measurements had suggested a bandgap value of about 1.89 eV at room temperature for this material [28], although it should be noted that these previous measurements were performed on powdered samples of InN [11, 28, 29, 30]. These new results suggest that InN, and that alloys of InN with GaN, can be used to fabricate a family of optical devices that span over a broad swath of the electromagnetic spectrum, ranging from the near-infrared to the ultraviolet regions [7]. This finding ignited tremendous interest in the material properties of the narrow-bandgap group-III nitride semiconductors.

Unfortunately, a major obstacle for the further development of the nitride based semiconductor device technologies remains the absence of a lattice matched substrate for the epitaxial growth of these materials. Presently, substrates, such as sapphire ($A1_2O_3$) and silicon carbide (SiC), are commonly used for the growth of high quality GaN films; it should be noted, however, that there has been great recent interest in the growth of GaN-based materials on silicon (Si) substrates, offering not only low production costs but also attractive opportunities to incorporate GaN-based electron devices into Si-based technologies [31, 32]. One of the major challenges in depositing GaN-based materials on any of these substrates is the large lattice mismatch between the substrate and GaN-based materials, which inhibits high quality crystal growth [32]. Therefore, a buffer layer, such as AlN, is often employed in order to ameliorate this problem. Intensive studies have been carried out to improve matters. Recently, an enhancement of InGaN film quality has been reported by Kurouchi *et al.* [33] with the insertion of a thin InN buffer layer. In another study, the film quality of InGaN was found to be improved when zinc oxide (ZnO) is used as the substrate instead of sapphire [34].

Mismatches between the growing epilayer and the underlying substrate lead to large concentrations of threading dislocation lines, i.e., between 10^7 and 10^{11} cm^{-2} [35, 36], these threading dislocation lines extending from the

substrate and/or buffer interface all the way into the deposited samples. In Figure 1.1, a typical transmission electron microscope image of the threading dislocation lines within InN is shown, this figure being from Cimalla *et al.* [37]. Dislocations are known to affect the electrical and the optical properties of semiconductors [38]. As a result, the study of the threading dislocation lines within group-III nitride semiconductors has been the focus of some attention in recent years. Electrically, it is known that within GaN, electrons trapped by the threading dislocation lines diminish the overall electron mobility [39, 40]. Optically, the trapping level associated with the dislocation defects can act as non-radiative recombination centers, and thus, are responsible for shaping features observed in the optical absorption and photoluminescence spectra [41].

In this thesis, the occupancy of the defect sites associated with the threading dislocation lines within GaN and InN will be examined. The way this occupancy shapes the material properties of these semiconductors will also be probed. The focus will be primarily upon those properties that have a direct impact upon electron device performance. The case of AlN is not considered as its energy gap is so wide that it effectively acts as an insulator and is thus electrically inert.

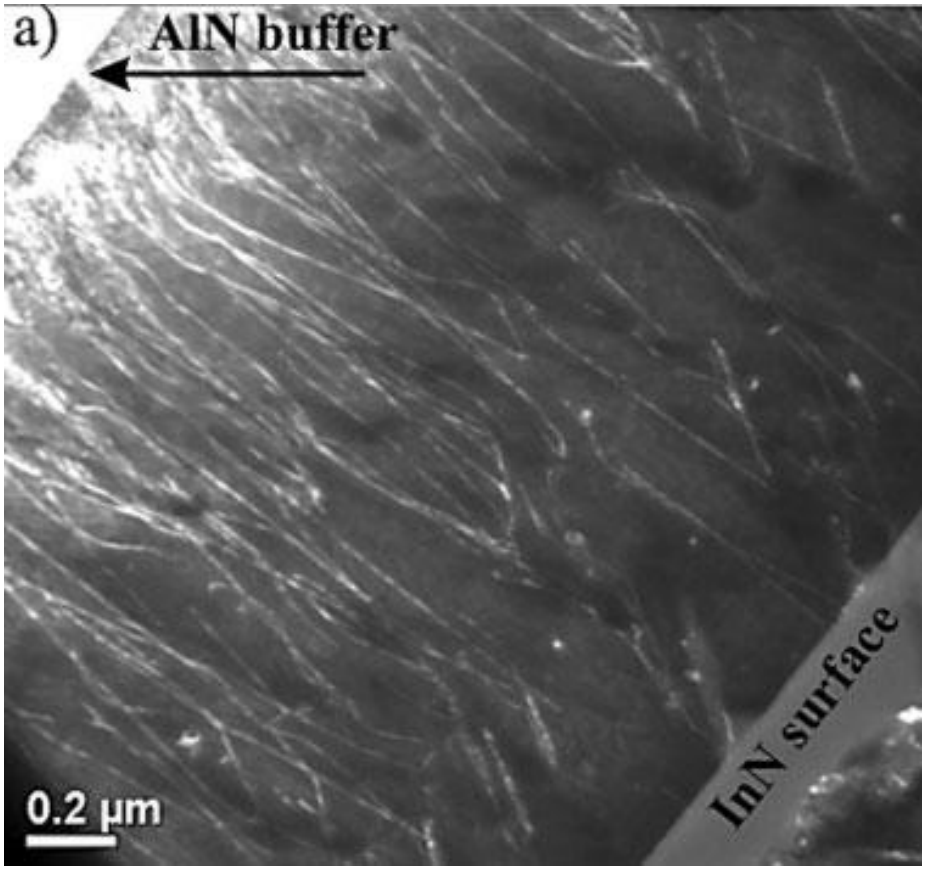

Figure 1.1: A transmission electron microscope image of the threading dislocation lines present within epitaxially grown InN. This image is from Cimalla *et al.* [37].

1.2 The crystalline structure of GaN and InN

Depending on the epitaxial growth conditions, GaN, InN, and related alloys, have been successfully grown in both the zinc-blende and the wurtzite crystal structures. In Figures 1.2(a) and (b), the atomic configurations associated with the zinc-blende and wurtzite crystal structures have been schematically depicted, respectively. The zinc-blende crystal structure can be thought of as being similar to the crystal structure associated with a diamond, with every other atom in the diamond crystal structure being replaced by an atom of the second element. The wurtzite crystal structure, however, is structurally closer to the graphite crystal structure. In order to distinguish the associated honey-comb meshes within the wurtzite crystal structure depicted in Figure 1.2(b), this crystal structure has to viewed from the top. The majority of work on GaN-based materials has been focused on the wurtzite structure, as most III-V nitride semiconductors have been grown epitaxially on sapphire substrates, resulting in wurtzite based nitride films [42, 43]. As a result, for the purposes of the analysis presented in this thesis, the focus will be on the electrical properties of the dislocation lines present within the wurtzite crystal structures associated with both GaN and InN.

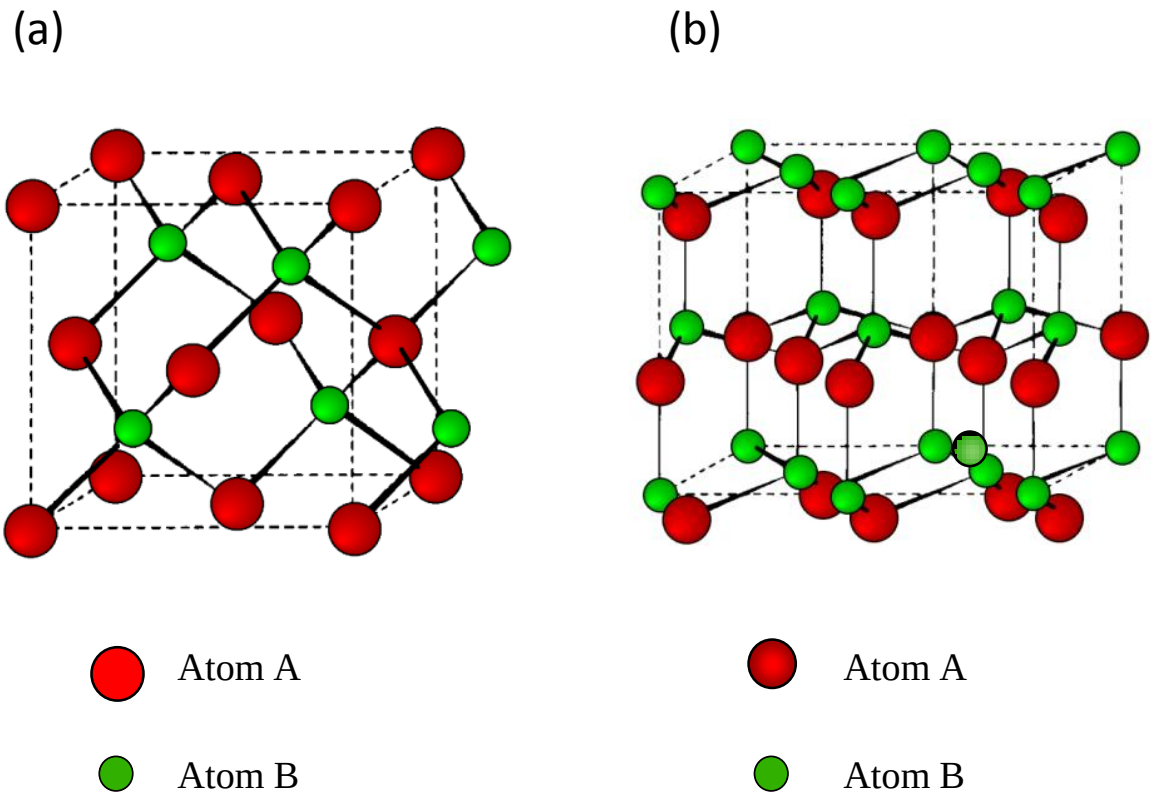

Figure 1.2: (a) The zinc-blende and (b) wurtzite crystal structures.

1.3 Material parameters associated with wurtzite GaN and wurtzite InN

In Table 1.1, the material parameters, corresponding to wurtzite GaN and wurtzite InN, are presented. The symbol, m_e, denotes the free electron mass.

Table 1.1: The material parameters corresponding to wurtzite GaN and wurtzite InN. These material parameters are drawn from the references indicated within the square brackets. The bulk donor energy levels are provided with respect to the valence band maximum.

Parameter	Symbol	GaN	InN
Electron effective mass	m_e^*	0.2 m_e [44]	0.04 m_e [45]
Energy gap	ε_g (eV)	3.4 [44]	0.7 [46]
Bulk donor energy level	ε_d (eV)	3.39 [47]	0.69 [48]
Relative dielectric constant	ϵ_r	8.9 [44]	15.3 [49]
c-lattice constant	c (Å)	5.1 [50]	5.71 [51]
a-lattice constant	a (Å)	3.16 [50]	3.53 [51]

1.4 Atomic structure of the edge type dislocations within the wurtzite GaN and wurtzite InN crystal structures

Dislocations are one dimensional defects embedded in the bulk of a crystal structure. Structurally, dislocations can be pure edge, pure screw, or of a mixed type. A schematic atomic configuration of such defects is depicted in Figure 1.3 [52]. Experimental results, presented in the literature, have shown that the majority of the dislocation lines within strained epitaxially grown samples of the nitride based semiconductors are pure edge in character [53, 54, 55, 56]. As a result, in this thesis, only edge type dislocations for the core structure of the dislocation lines will be considered. Several different atomic configurations, for the core structure of edge type dislocations within the wurtzite crystal structure of GaN, have been suggested in the literature [57, 58]. These include the 4-ring, the 5/7-ring, the 8-ring, the gallium vacancy, and the nitrogen vacancy dislocation core structures. The 5/7-ring and the 8-ring core structures have alternatively been referred to as the open core and full core dislocations, respectively.

The defect site associated with each of these dislocation core structures is depicted in Figure 1.4. Parts (a), (b), and (c) of this figure are after Takie

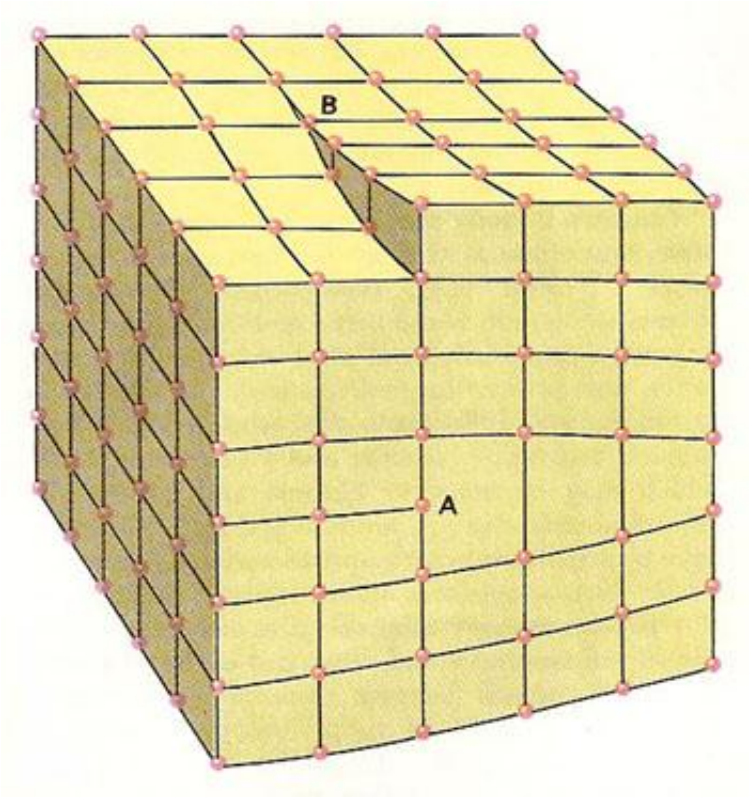

Figure 1.3: A section of a cubic crystal lattice, including a pure edge (A) and a pure screw dislocation (B). This figure is from Darling [52].

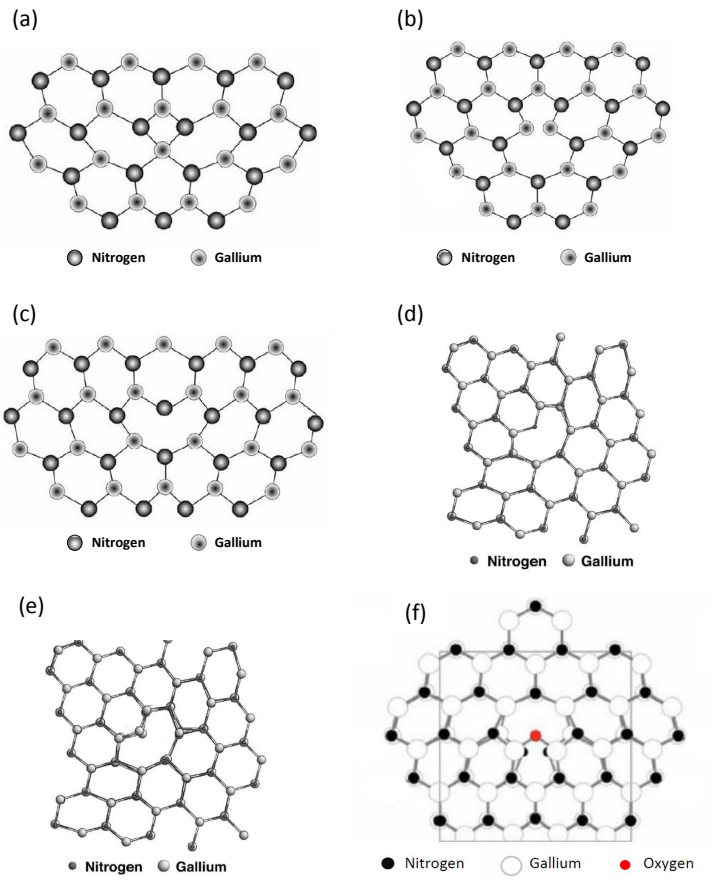

Figure 1.4: Schematic atomic configurations of the: (a) 4-ring, (b) 5/7-ring, (c) 8-ring, (d) gallium vacancy, (e) nitrogen vacancy, and (f) $V_{Ga} - O_N$ dislocation core structures within wurtzite GaN. Parts (a), (b), and (c) are after Takie and Nakayama [59]. Parts (d) and (e) are after Lee *et al.* [57]. Part (f) is after You *et al.* [60].

and Nakayama [59], while parts (d) and (e) are after Lee *et al.* [57]. Part (f) is after You *et al.* [60]. The wurtzite lattice c-direction, along with the [0001] crystallographic growth direction, runs out of the page for all parts of Figure 1.4. Similar dislocation core structures have also been suggested for the threading dislocation lines within wurtzite InN [59, 61].

Of particular importance in this thesis, is another dislocation core structure within the wurtzite crystal structure of GaN, depicted in Figure 1.4(f), and henceforth referred to as the $V_{Ga} - O_N$ dislocation core structure. This dislocation core structure can be obtained from the gallium vacancy dislocation core structure through the replacement of the nitrogen atom at the center of the gallium vacancy dislocation core structure with an oxygen atom. In Section 4.6, the energy configuration, as well as the occupation statistics associated with the $V_{Ga} - O_N$ dislocation core structure, will be discussed in greater detail.

Regardless of the particular atomic configuration of the dislocation core structure, in this thesis, the smallest repetitive structural unit of the dislocation, along the direction of the dislocation line, will henceforth be referred to as a dislocation defect site.

1.5 Electrical properties of the threading dislocation lines within GaN and InN

Dislocation lines within semiconductors were identified as possessing electrical properties associated with them as early as the 1950s [62, 63]. It was observed that after the introduction of dislocations through plastic deformation into samples of n-doped germanium and silicon, the free electron concentration, as well as the overall electron mobility, decreased measurably within these semiconductor materials. A thorough review article on the electrical, as well as the optical properties of dislocations within germanium and silicon, exists in the literature [64].

Within GaN and InN, it has also been observed that the electron mobility is adversely affected by the presence of the threading dislocation lines [39, 40, 65, 66, 67]. Studies suggest that the threading dislocation lines affect the free electron concentration of the associated semiconductor material differently within n-type GaN and n-type InN; within n-type GaN, experimental results, obtained from the electron holographic mapping of individual threading dislocation lines, have shown the dislocation defect sites to be negatively charged [68, 69, 70, 71]. In other words, within GaN, the dislocation defect sites act to reduce the free electron concentration of the material by trap-

ping some fraction of the free electrons from the conduction band. Within n-type InN, however, several investigations suggest that the threading dislocation lines contribute to the problem of the unintentional n-type nature of this semiconductor material [59, 61, 66, 72]. In other words, within InN, the dislocation defect sites donate electrons to the conduction band, thereby increasing the free electron concentration within this semiconductor material. The underlying reason for this difference in the contribution of the threading dislocation lines to the free electron concentration within GaN and InN, is the difference in the positioning of the dislocation defect energy level, ε_t, with respect to the conduction band minimum for each case. Within GaN, the dislocation defect energy level lies deep within the energy gap. In the case of InN, however, the dislocation defect energy level is suggested to lie above the conduction band minimum.

Several approaches have been pursued in the literature in order to determine the occupancy of the dislocation defect sites within n-type GaN. The earliest modeling of the charge build up along a dislocation line is due to Read [73]. The model of Read remains the most widely used model for the treatment of the occupancy of the dislocation lines within semiconductors to date. The model of Read [73] pictures a dislocation line within the diamond crystal structure of germanium as being comprised of a row of identical and

equally spaced dangling bonds; see Figure 1.5.

A revised electrostatic theory of charged dislocation lines within semiconductors has been formulated in this thesis. In addition to the screening space charge distribution profile, this procedure also gives a computational solution to the electrostatic potential surrounding the charged dislocation lines. The electrostatic potential thus obtained enables a determination of the electron mobility limited by scattering from the charged dislocation lines with greater certainty than that which has previously been achieved in the literature. In addition, the development of theoretical tools, that may be more easily applied to such problems, has been a focus of study. The nature of the screening mechanisms within these materials is also examined. Ultimately, fresh insights into the nature of these charged defects, and how they may influence the performance of GaN and InN related electron devices, have been acquired.

This thesis is organized in the following manner. In Chapter 2, a formulation for obtaining the most general screening space charge distribution surrounding a dislocation line within a semiconductor will be developed. Then this formulation will be applied to the specific case of dislocation lines within GaN and InN. In particular, it will be shown that distinctively different screening space charge distribution profiles exist around the threading

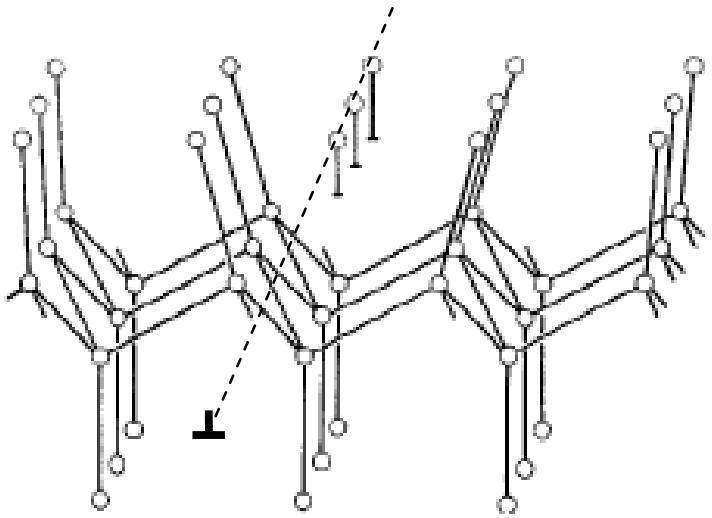

Figure 1.5: The atomic structure of a dislocation line within the diamond crystal structure. This figure is after Read [73]. The direction of the dislocation line is indicated with the dashed line in this figure. The symbol $\perp$ is frequently used in order to denote an edge type dislocation in the literature.

dislocation lines within GaN and InN. In Chapter 3, the formulation for electron scattering from charged dislocation lines will be presented. Both the electron drift and Hall mobilities, limited by scattering from the threading dislocation lines within GaN and InN, will be computed. In Chapter 4, the dislocation occupation statistics will be discussed. In particular, it is suggested that a Gibbs factor formalism can be used to obtain the occupation statistics of the defect sites along threading dislocation lines within a semiconductor. Finally, conclusions are drawn in Chapter 5 and recommendations for future research are made.

Chapter 2

Dislocation line charge screening

2.1 Modeling the charge build-up along the dislocation lines

As was mentioned in the previous chapter, the defect sites along the threading dislocation lines within GaN and InN can be electrically active. Taking charge neutrality considerations into account, a negative or positive charge residing on the defect sites along threading dislocation lines should be compensated by a spatial charge distribution of the opposite polarity

and equal in magnitude surrounding each threading dislocation line. This surrounding space charge distribution will henceforth be referred to as the screening space charge distribution.

In this thesis, for computational simplicity, the screening space charge distribution will be assumed to be invariant along the direction of the dislocation lines. As a result, in cylindrical coordinates, a solely radial functional form will be assumed for the screening space charge distribution. This invariance assumption is valid if (1) the dislocation lines are infinitely long, and (2) the discrete charge residing at the defect sites along these dislocation lines can be modeled with a uniform linear charge along the lines. In order to avoid the electrostatic potential surrounding the dislocation lines from becoming singular at $r = 0$, the core charge distribution will be considered to be spread uniformly in a cylinder of radius, R_{dc}, which will henceforth be referred to as the dislocation core radius.

For the purposes of this analysis, the basal lattice constant, a, in the wurtzite crystal structures of GaN and InN will be taken as the dislocation core radius, R_{dc}, for each case. As a result, in this chapter, the charge build-up at each threading dislocation line will be modeled with two coaxial, infinitely long, space charge cylinders, as shown in Figure 2.1. The threading dislocation lines extend in the [0001] crystallographic direction of the wurtzite

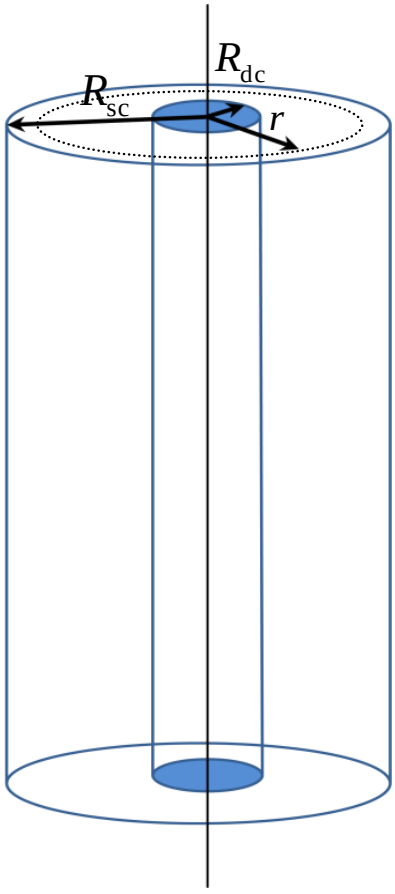

Figure 2.1: Modeling the space charge build-up around a threading dislocation line. R_{dc} denotes the dislocation core radius. R_{sc} represents the screening space charge cylinder radius. R_{sc} will be introduced subsequently.

crystal structure for both GaN and InN.

The question as to whether the defect sites along the dislocation lines within a given semiconductor material become predominantly positively or negatively charged depends upon (1) the positioning of the dislocation defect energy level, ε_t, within the energy band structure of the semiconductor material, and (2) the bulk doping conditions of the semiconductor material. For the purposes of this analysis, the primary focus is on n-type bulk doping conditions of the semiconductor material; it is experimentally observed that most samples of GaN and InN are n-type doped in nature [66, 72]. It has been suggested that within GaN, the dislocation defect sites introduce a deep acceptor level within the energy gap of GaN. As a result, the dislocation defect sites within GaN have a natural tendency to accept electrons, thereby becoming negatively charged. This situation is schematically depicted in Figure 2.2. Within InN, however, the dislocation defect energy level, ε_t, has been shown in the literature to lie above the conduction band minimum [59, 61]. As a result, the dislocation defect sites within InN have a natural tendency to donate their electrons to the conduction band and thereby become positively charged. This situation is schematically depicted in Figure 2.3.

In this chapter, a quantitative analysis of the screening space charge distribution surrounding a threading dislocation line is presented. The analysis

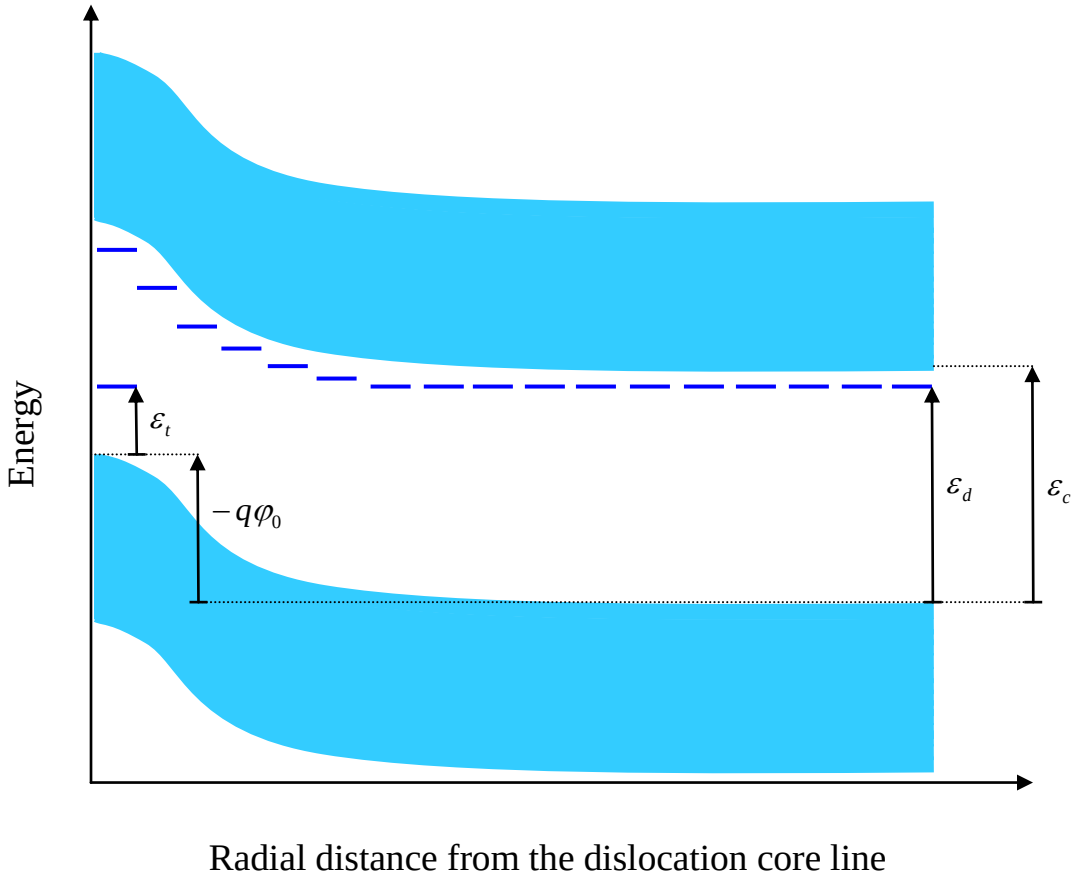

Figure 2.2: Schematic diagram for the energy band bending around a threading dislocation line within GaN.

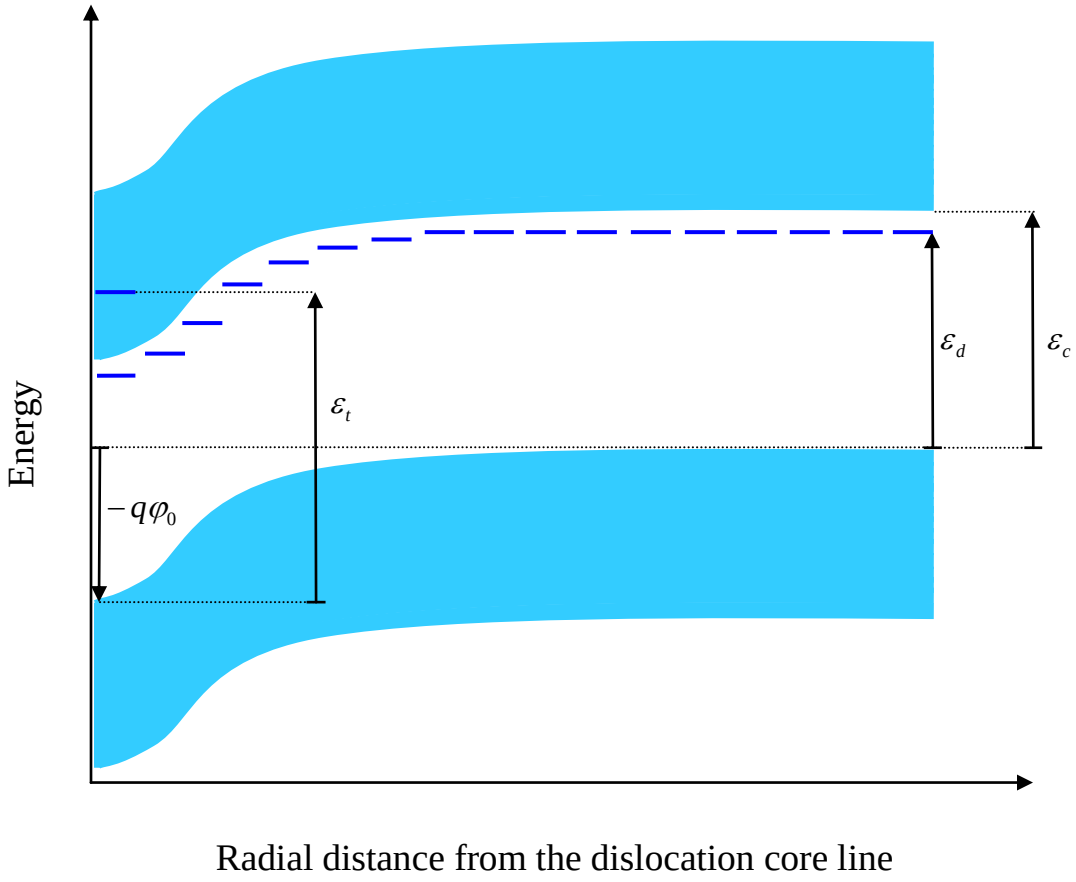

Figure 2.3: Schematic diagram for the energy band bending around a threading dislocation line within InN.

is cast within the framework of the aforementioned radial spatial charge distribution assumption. Following the presentation of a general formulation for this problem, the dislocation line charge screening, specific to GaN and InN, are then computed. The analyzes presented in the subsequent chapters will be built upon the framework of the formulation developed in this chapter.

This chapter is organized in the following manner. In Section 2.2, a general formulation for the screening of the dislocation lines within a semiconductor material will be developed. Then, in Section 2.3, this formulation will be applied to the specific case of n-type GaN in order to obtain the screening space charge distribution, as well as the associated electrostatic potential function, surrounding the threading dislocation lines within this semiconductor. In Section 2.4, the electrostatic potential obtained from this formulation will be compared with existing electron holographic experimental data in the literature. In Section 2.5, the formulation will be applied to the specific case of n-type InN.

2.2 Formulating the screening space charge distribution surrounding a dislocation line

In modeling the space charge distribution associated with a dislocation line, it is useful to treat the charge accumulated on the defect sites along the core of the dislocation line with a uniform space charge of constant concentration, $N_{\rm dc}$, confined to an inner cylinder of radius $R_{\rm dc}$, i.e.,

$$n_{\rm dc}(r) = \begin{cases} N_{\rm dc}, & r \leq R_{\rm dc} \\ 0, & r > R_{\rm dc} \end{cases} . \tag{2.1}$$

This space charge cylinder will henceforth be referred to as the dislocation core charge cylinder. Assuming that the dislocation defect sites are separated by the c-lattice constant associated with the relevant wurtzite crystal structure, c, and denoting the charge donated per dislocation defect site along a dislocation line by f, the constant dislocation core space charge concentration, $N_{\rm dc}$, in units of the fundamental electron charge, q, can thus be expressed as

$$N_{\rm dc} = \frac{f}{\pi R_{\rm dc}^2 c}. \tag{2.2}$$

Surrounding each dislocation core charge cylinder is a screening space charge cylinder of the opposite charge. For computational convenience, the radius of this space charge cylinder, $R_{\rm sc}$, will be assumed to be finite. Under predominantly n-type bulk doping conditions, the contributions from the

bulk acceptor and bulk hole concentrations to this screening space charge concentration can be neglected. Thus, the screening space charge concentration, $n_{\rm sc}(r)$, in units of the fundamental electron charge, q, may be written as

$$n_{\rm sc}(r) = \begin{cases} n(r) - N_{\rm d}^{+}(r), & r \leq R_{\rm sc} \\ 0, & r > R_{\rm sc}. \end{cases} . \tag{2.3}$$

In this equation, $N_{\rm d}^{+}(r)$ and $n(r)$ represent the bulk ionized donor and free electron concentrations, respectively, at a radial distance, r, from the dislocation line core center.

Poisson's equation may be expressed as

$$\nabla^2 \varphi = -\frac{\rho}{\epsilon_r \epsilon_0}, \tag{2.4}$$

where ϵ_r denotes the relative dielectric constant of the material, ϵ_0 represents the dielectric constant associated with free space, and ρ is the space charge concentration. Within the framework of cylindrical coordinates,

$$\nabla^2 \varphi = \frac{1}{r}\frac{\partial}{\partial r}\left(r\frac{\partial \varphi}{\partial\, r}\right) + \frac{1}{r^2}\frac{\partial^2 \varphi}{\partial \phi^2} + \frac{\partial^2 \varphi}{\partial z^2}, \tag{2.5}$$

and thus, Eq. (2.4) can be written as

$$\frac{1}{r}\frac{\partial}{\partial r}\left(r\frac{\partial \varphi}{\partial\, r}\right) + \frac{1}{r^2}\frac{\partial^2 \varphi}{\partial \phi^2} + \frac{\partial^2 \varphi}{\partial z^2} = -\frac{\rho}{\epsilon_r \epsilon_0}. \tag{2.6}$$

A cylindrical spatial charge distribution associated with a dislocation line implies a cylindrically symmetric electrostatic potential. That is, within the

present framework of the dislocation line charge modeling, $\varphi(r)$ does not depend on the ϕ and z coordinates. As a result, Eq. (2.6) further reduces to

$$\frac{1}{r}\frac{\partial}{\partial r}\left(r\frac{\partial\varphi(r)}{\partial\, r}\right) = -\frac{\rho}{\epsilon_r\epsilon_0}. \tag{2.7}$$

Noting that the space charge concentration associated with a given threading dislocation line may be expressed as the difference between the core space charge concentration and the screening space charge concentration, i.e.,

$$\rho = q(n_{\rm dc} - n_{\rm sc}), \tag{2.8}$$

Eq. (2.7) can be integrated to obtain the resultant electrostatic potential

$$\varphi(r) = -\frac{q}{\epsilon_r\epsilon_0}\int_0^r \frac{1}{r'}\int_0^{r'} r''\left[n_{\rm dc}(r'') - n_{\rm sc}(r'')\right]\, dr''\, dr' + c_{\rm int}, \tag{2.9}$$

where $c_{\rm int}$ is a constant of integration that will ultimately be determined through the requirement that $\varphi(r \geq R_{\rm sc}) = 0$.

The effect of the electrostatic potential, $\varphi(r)$, in the neighbourhood of the dislocation core is to shift all of the electronic energy levels by the amount $-q\varphi(r)$ relative to the Fermi energy level, $\varepsilon_{\rm F}$. For the bulk ionized donor and free electron concentrations employed in Eq. (2.3), this can be achieved by expressing

$$N_{\rm d}^{+}(r) = \frac{N_{\rm d}}{1 + 2\exp\left[\left(\varepsilon_{\rm F} - \left(\varepsilon_d - q\varphi(r)\right)\right)/kT\right]}, \tag{2.10}$$

and

$$n(r) = N_c \frac{2}{\sqrt{\pi}} \int_0^\infty \frac{\sqrt{x}}{1 + \exp\left[x - (\varepsilon_{\mathrm{F}} - (\varepsilon_c - q\varphi(r)))/kT\right]} \, \mathrm{d}x, \tag{2.11}$$

where ε_d and ε_c denote the bulk donor and conduction band minimum energy levels, respectively. N_{d} represents the bulk donor concentration and N_c denotes the effective density of states of the conduction band, i.e.,

$$N_c \equiv 2 \left(\frac{m_c^* kT}{2\pi\hbar^2} \right)^{3/2}, \tag{2.12}$$

m_c^*, k, $\hbar$, and T being the electron effective mass, Boltzmann's constant, the reduced Planck's constant, and the temperature, respectively.

The position of the Fermi energy level, ε_{F}, can be obtained from the local charge neutrality condition at distances far from the dislocation lines, where the potential, $\varphi(r)$, reduces to zero. That is

$$N_c \frac{2}{\sqrt{\pi}} \int_0^\infty \frac{\sqrt{x}}{1 + \exp\left[x - (\varepsilon_{\mathrm{F}} - \varepsilon_c)/kT\right]} \, \mathrm{d}x = \frac{N_{\mathrm{d}}}{1 + 2\exp\left[(\varepsilon_{\mathrm{F}} - \varepsilon_d)/kT\right]}. \tag{2.13}$$

It is seen that Eq. (2.13) is simply equivalent to saying that $n_{\mathrm{sc}}(r) = 0$, which should be the case at distances far from the dislocation lines, i.e., for $r \geq R_{\mathrm{sc}}$.

In the present analysis, the space charge concentration, $n_{\mathrm{sc}}(r)$, and the electrostatic potential, $\varphi(r)$, will be taken as the unknown variables of the formulation. In order to simultaneously solve for $n_{\mathrm{sc}}(r)$ and $\varphi(r)$ from Eqs. (2.3)

and (2.9), an iterative approach will be proposed that involves finding successively more accurate solutions to the screening space charge distribution function, $n_{sc}(r)$. The details of this iterative approach, for the cases of GaN and InN, are provided in Appendices A and B, respectively.

2.3 Threading dislocation line charge screening within GaN

The screening space charge concentration profile, $n_{sc}(r)$, and the corresponding electrostatic potential function, $\varphi(r)$, within GaN are plotted as a function of the radius, r, for five different values of the negative charge donated per dislocation defect site, f, in Figures 2.4 and 2.5, respectively. The bulk donor concentration has been fixed to $10^{18}\,\mathrm{cm}^{-3}$ for all of the curves depicted in these figures. The GaN material parameters used in obtaining these results are specified in Table 1.1. The radius of the dislocation core charge cylinder has been set equal to the basal lattice constant of the wurtzite crystal structure of GaN, a, i.e., 3.16 Å. The corresponding calculations are all performed at 300 K.

The results presented in Figures 2.4 and 2.5 warrant the following observations:

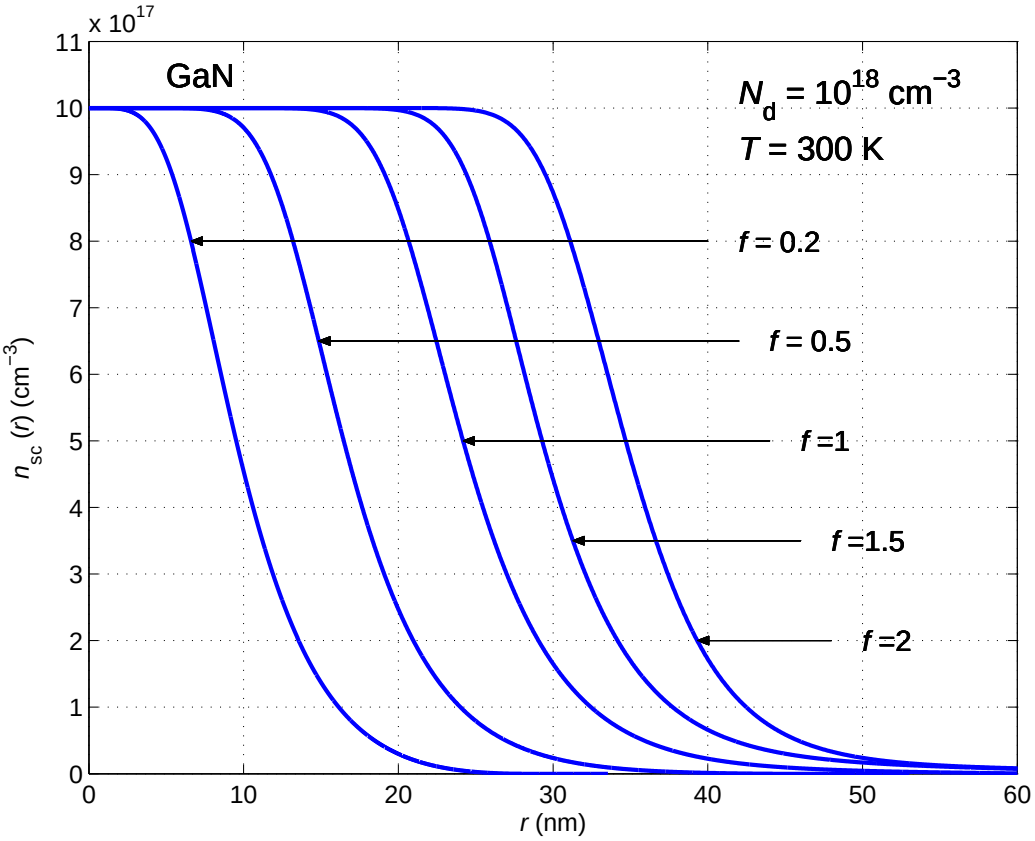

Figure 2.4: The screening space charge concentration of a threading dislocation line within GaN. The bulk donor concentration, N_d, is set to $10^{18}\,\mathrm{cm}^{-3}$ and the temperature set to 300 K for the purposes of this analysis.

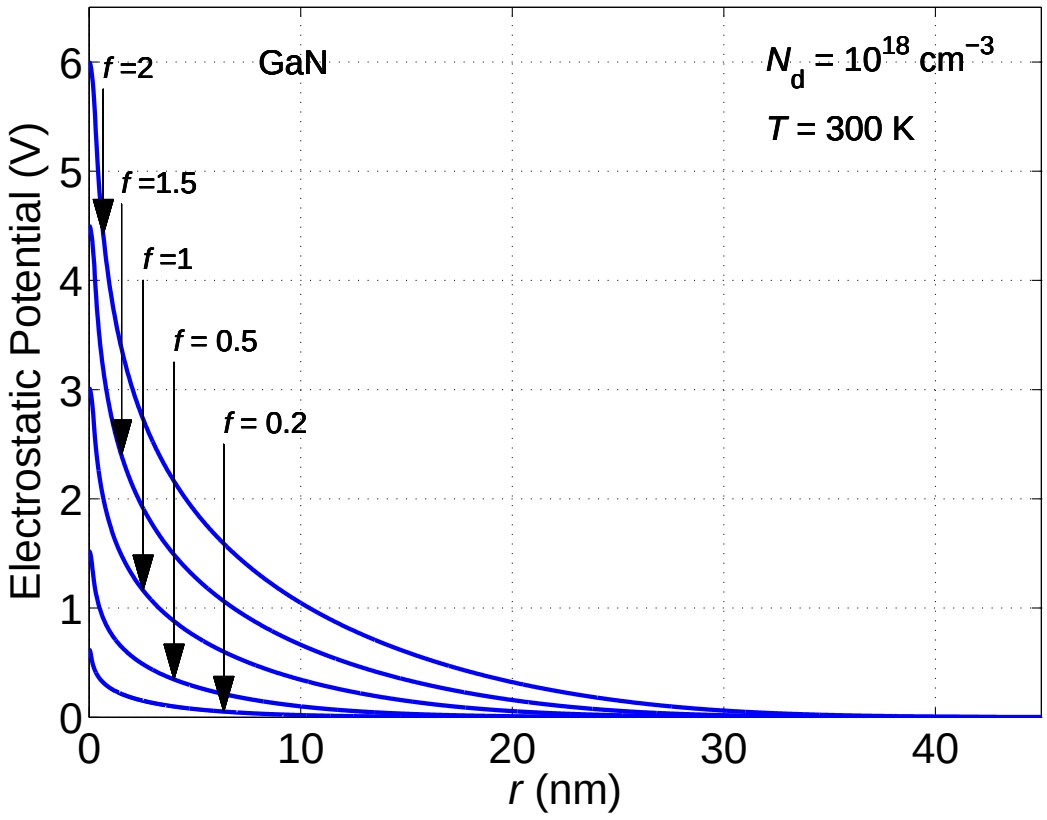

Figure 2.5: The magnitude of the electrostatic potential surrounding a threading dislocation line within GaN. The bulk donor concentration, N_d, is set to $10^{18}\,\mathrm{cm}^{-3}$ and the temperature set to 300 K for the purposes of this analysis.

- it is observed that with increased values of f, more and more of the bulk donor atoms at larger radial distances from the dislocation core loose their donated electrons to the defect sites along the threading dislocation lines

- due to the requirement of charge neutrality around each threading dislocation line, the positive charge contained within the screening space charge distribution, $n_{\rm sc}(r)$, is directly proportional to the value of f, i.e.,

$$f \propto \int_0^{R_{\rm sc}} n_{\rm sc}(r) 2\pi r \, {\rm d}r, \tag{2.14}$$

  for each curve depicted in Figure 2.4

- close to the dislocation line, the screening space charge concentration reaches its maximum possible value of $10^{18}\,{\rm cm}^{-3}$; however, as we start to move away from the dislocation line, it is observed that screening from free electrons gradually reduces the screening space charge concentration to zero at large radial distances from the dislocation line.

2.4 Comparison with experiment

Off-axis electron holography is an interferometric technique that can measure the phase shift in an electron wave passing through an object. Since

the phase shift in the electron wave function is sensitive to the local electrostatic potential within the sample, electron holography can be used to provide quantitative information about potential variations with nanometer-scale resolution. The electrostatic potential associated with a charged dislocation line within wurtzite GaN has been experimentally determined by Cherns *et al.* [69]; through the use of electron holography, Cherns *et al.* [69] experimentally determined the electrostatic potential associated with an individual threading dislocation line within n-type wurtzite GaN. Their experimental results are presented in Figure 2.6. For the bulk doping concentration found by Cherns *et al.* [69], i.e., $N_{\rm d} = 6 \times 10^{17}$ cm^{-3}, a satisfactory fit to this experimental data may be achieved through the present analysis by setting the negative charge donated per dislocation defect site to two, i.e., $f = 2$. This best fit from the reults of the present analysis is also depicted in Figure 2.6.

2.5 Threading dislocation line charge screening within InN

Using the formulation developed in Section 2.2, the screening space charge concentration profile, $n_{\rm sc}(r)$, and the corresponding electrostatic potential function, $\varphi(r)$, within InN are plotted as a function of the radius, r,

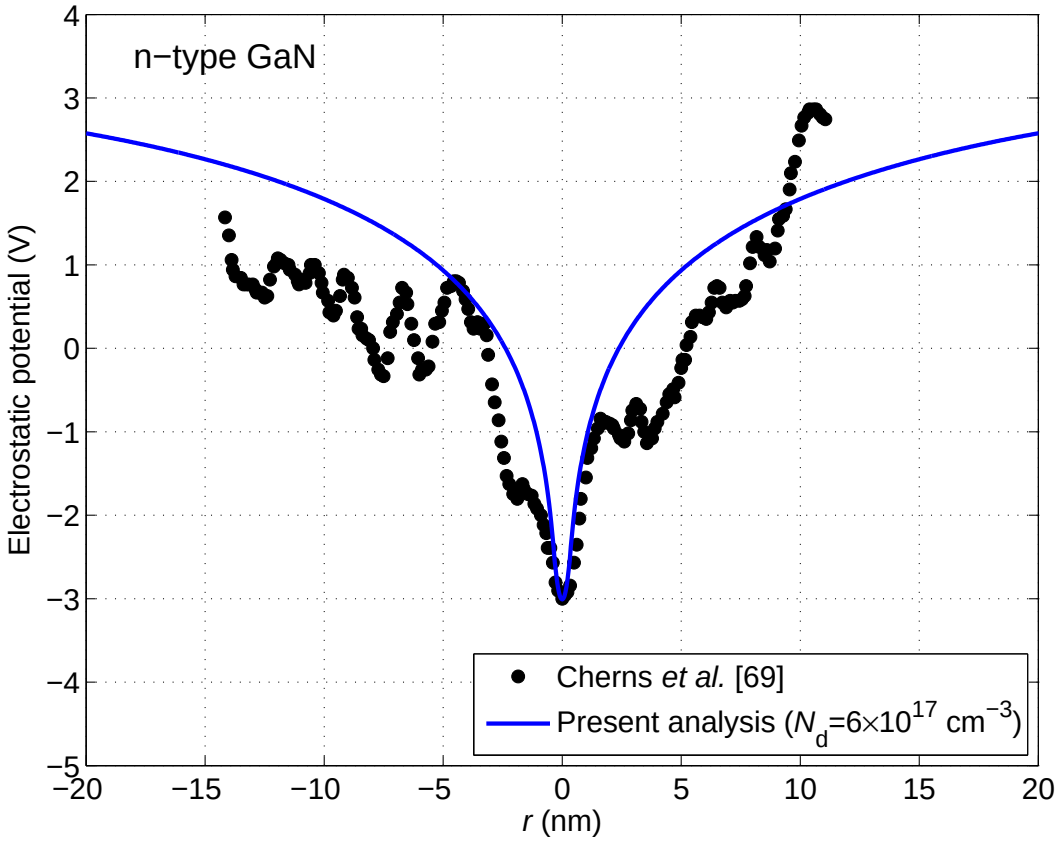

Figure 2.6: Comparison of the results from the present analysis with the experimental data of Cherns *et al.* [69]. For this analysis, f is set to 2 and the bulk doping concnetration, N_{d}, is set to 6×10^{17} cm^{-3}, this being the value measured by Cherns *et al.* [69].

for different values of the negative charge donated per dislocation defect site, f, in Figures 2.7 and 2.8, respectively. Similar to the computations for the case of GaN, the bulk donor concentration has been fixed to $10^{18}\,\mathrm{cm}^{-3}$ for all of the curves depicted in these figures. The InN material parameters used for these computations are specified in Table 1.1. The radius of the dislocation core charge cylinder has been set equal to the basal lattice constant of the wurtzite crystal structure of InN, a, i.e., 3.53 Å. The corresponding calculations are all performed at 300 K.

The results presented in Figures 2.7 and 2.8 warrant the following observations:

- it is observed that with increasing values of f, the screening space charge concentration increases rapidly at distances close to the dislocation line

- due to the requirement of charge neutrality around each of the threading dislocation lines, the negative charge contained within the screening space charge distribution, $n_{\mathrm{sc}}(r)$, is directly proportional to the value of f, i.e.,

$$f \propto \int_0^{R_{\mathrm{sc}}} n_{\mathrm{sc}}(r) 2\pi r \,\mathrm{d}r, \tag{2.15}$$

  for each curve depicted in Figure 2.7

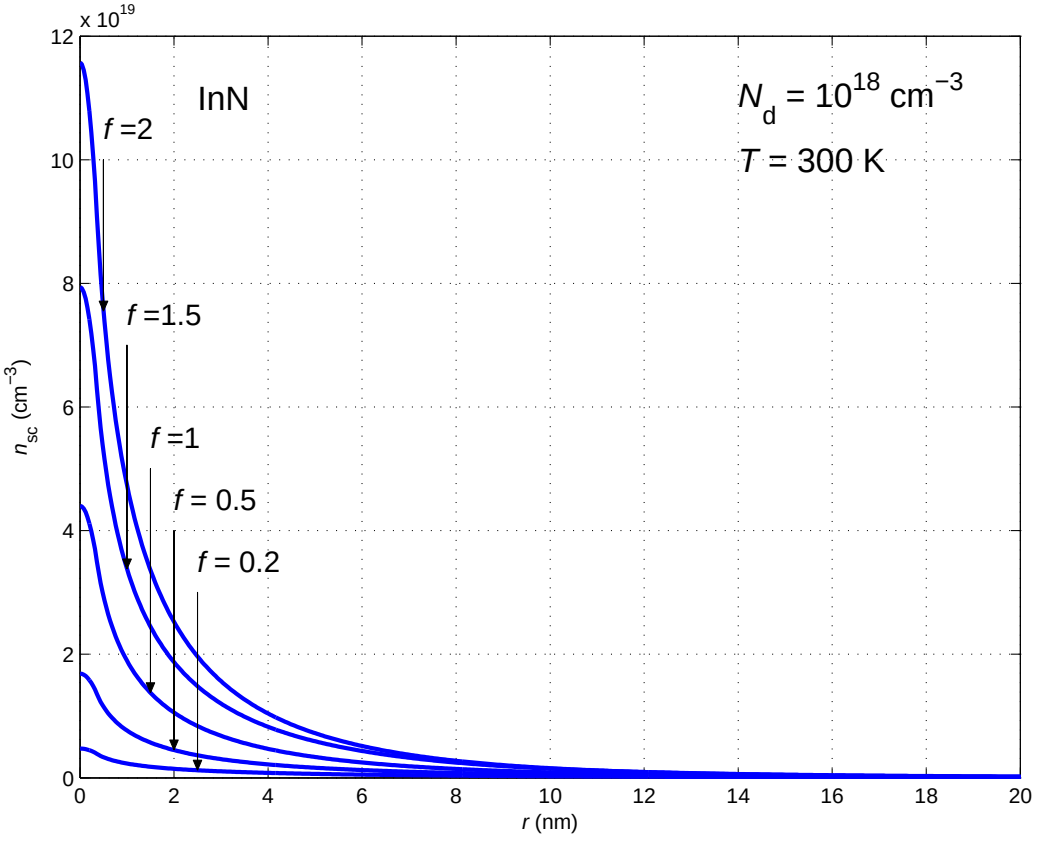

Figure 2.7: Screening space charge concentration of a threading dislocation line within InN. The bulk donor concentration, N_d, is set to $10^{18}\,\mathrm{cm}^{-3}$ and the temperature set to 300 K for the purposes of this analysis.

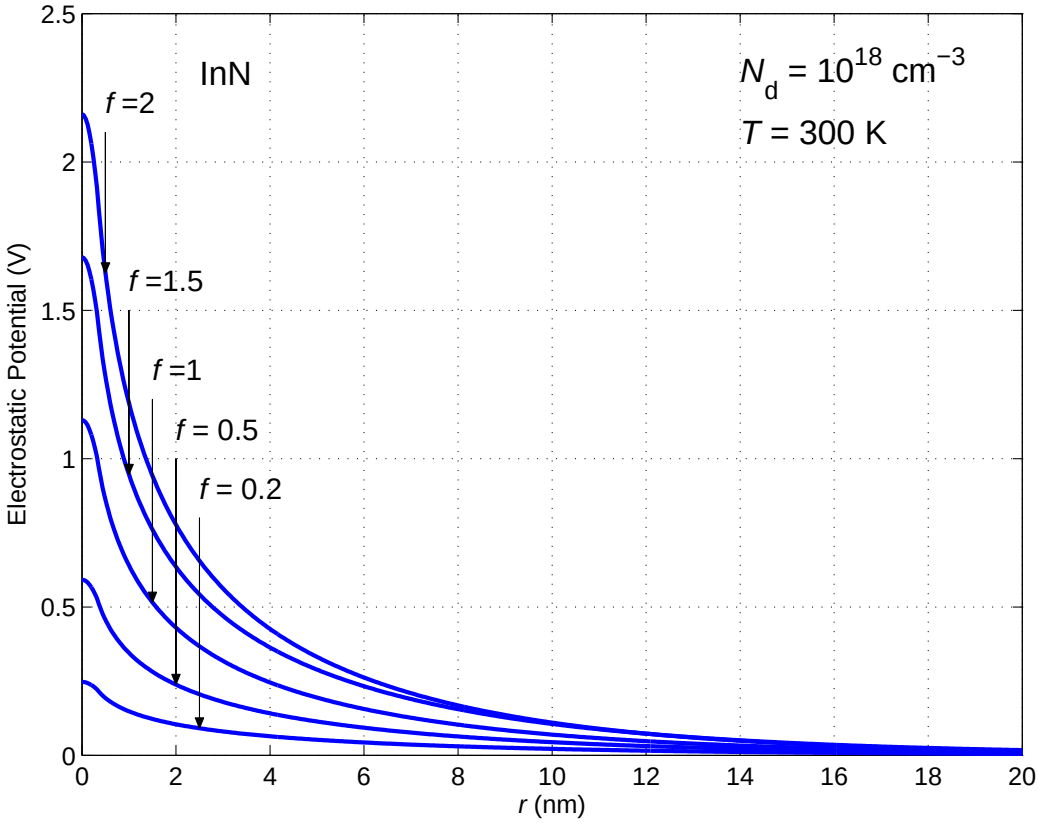

Figure 2.8: The magnitude of the electrostatic potential surrounding a threading dislocation line within InN. The bulk donor concentration, N_d, is set to $10^{18}\,\mathrm{cm}^{-3}$ and the temperature set to 300 K for the purposes of this analysis.

- unlike what was seen in the screening of the dislocation core charge within GaN, within InN the screening close to the dislocation line is provided predominantly by free carriers.

This free carrier screening constitutes a much more effective screening of the dislocation core charge when compared with the screening of the dislocation core charge offered by the ionized donors present within GaN. As a result, it is seen that for the same value of f, the values for the computed electrostatic potential function, $\varphi(r)$, are much lower within InN than for the case of GaN; compare Figures 2.5 and 2.8.

Chapter 3

Electron mobility limited by scattering from charged dislocation lines

3.1 The electron drift and Hall mobilities in semiconductors

The electron mobility characterizes how quickly an electron can move through a material under the action of an applied electric field. When an electric field, $\mathcal{E}$, is applied across a piece of a semiconductor material, the

electrons respond by moving with an average velocity, v^{drift}, referred to as the electron drift velocity. Within a given semiconductor material, the electron mobility depends on the magnitude of the electric field, particularly at high fields, when velocity saturation occurs. In the present thesis, however, the focus is on low-field electron mobilities.

At low applied electric field strengths, the electron drift velocity is linearly proportional to the applied electric field strength. That is

$$v^{\text{drift}} = -\mu^{\text{drift}}\mathcal{E}, \tag{3.1}$$

where μ^{drift} denotes the electron drift mobility and the negative sign reflects the fact that electrons are pulled in the opposite direction of the applied electric field. Electron mobilities are almost always specified in units of cm^2/Vs.

The electron mobility arises as a consequence of imperfections within a semiconductor material and as a result of the interaction of transiting electrons with the atoms within the material, which naturally engage in vibrations as a result of thermal processes. Each material system possesses crystal defects, vacancies, dislocations, impurities, and other features which will act to scatter transiting electrons. At elevated temperatures, due to their thermal energy, the atoms within the crystal structure of a semiconductor material will vibrate about their equilibrium lattice sites. The transiting electrons will collide with such vibrating atoms, and, as a result, will be scattered.

As with the molecules of a gas within a container, in the absence of an applied electric field, the conducting electrons within a semiconductor material move in random directions, with a wide range of different energies. When an electric field is applied, a net average velocity is obtained, this velocity being in the opposite direction of the applied electric field. The average time it takes for an electron within a semiconductor material to move between successive scattering events is denoted by $\langle \tau \rangle$. The bracket notation in this expression, $\langle \tau \rangle$, is used to denote an averaging over all possible energies of the incident electron. In the literature, the physical quantity, $\langle \tau \rangle$, is often referred to as the mean free time, or the relaxation time, of the electrons.

Under the action of an applied electric field, $\mathcal{E}$, electrons will accelerate at a rate equal to $-q\mathcal{E}/m_e^*$ between the successive scattering events. Noting that the force exerted on an electron by the periodic net positive charge of the lattice atoms is already implicitly contained within the electron effective mass term, m_e^*, the electron drift velocity can thus be expressed as

$$v^{\text{drift}} = -\frac{q\mathcal{E}}{m_e^*} \langle \tau \rangle \,. \tag{3.2}$$

That is, on average, an electron's velocity in the opposite direction of the applied electric field is proportional to the product of the applied electric field strength and the average time between scattering events, and inversely proportional to the electron effective mass. A comparison of Eq. (3.2) with

Eq. (3.1), gives the following expression for the electron drift mobility

$$\mu^{\text{drift}} = \frac{q\langle\tau\rangle}{m_e^*}. \tag{3.3}$$

Empirically, electron mobility is often measured through the use of a Hall effect experiment. In the Hall effect experiment, in addition to the applied electric field, $\mathcal{E}$, the transport of the conduction electrons is affected by the presence of a weak magnetic field, B, applied in a direction perpendicular to that of the applied electric field. As a result, the experimentally measured electron Hall mobility differs slightly from the electron drift mobility defined earlier. Specifically, it can be shown that the electron Hall mobility is related to the electron drift mobility through the following relationship

$$\mu^{\text{Hall}} = \frac{\langle\tau^2\rangle}{\langle\tau\rangle^2}\mu^{\text{drift}}, \tag{3.4}$$

where, once again, the bracket notation in the expressions for $\langle\tau^2\rangle$ and $\langle\tau\rangle$, represents an averaging of the relaxation time squared and the relaxation time over all of the possible energies of the incident wave vectors [74].

For multiple scattering mechanisms, the effective mean free time is derived from the individual mean free times of the representative scattering events, i.e.,

$$\frac{1}{\langle\tau\rangle} = \frac{1}{\langle\tau_{\text{dis}}\rangle} + \frac{1}{\langle\tau_{\text{imp}}\rangle} + \frac{1}{\langle\tau_{\text{piezo}}\rangle} + \frac{1}{\langle\tau_{\text{lattice}}\rangle} + ..., \tag{3.5}$$

where $\langle\tau_{\text{dis}}\rangle$, $\langle\tau_{\text{imp}}\rangle$, $\langle\tau_{\text{piezo}}\rangle$, and $\langle\tau_{\text{lattice}}\rangle$ denote the dislocation scattering limited mean free time, the impurity scattering limited mean free time, the piezoelectric scattering limited mean free time, and the lattice vibration scattering limited mean free time, respectively. Multiplying both sides of Eq. (3.5) by m_e^*/q, one obtains the celebrated Matthiessen's rule, relating the overall electron mobility, μ, to the partial electron mobilities, i.e.,

$$\frac{1}{\mu} = \frac{1}{\mu_{\text{dis}}} + \frac{1}{\mu_{\text{imp}}} + \frac{1}{\mu_{\text{piezo}}} + \frac{1}{\mu_{\text{lattice}}} + ..., \tag{3.6}$$

where μ_{dis}, μ_{imp}, μ_{piezo}, and μ_{lattice} denote the dislocation limited, impurity limited, piezoelectric limited, and lattice vibration limited electron mobilities, respectively. It should be mentioned that Matthiessen's rule is an approximation and is not universally valid. This rule is not valid if the factors affecting the mobility depend on each other, because individual scattering probabilities cannot be summed unless they are independent of each other.

Among the different electron scattering mechanisms present within GaN and InN, in this thesis, only the electron drift and Hall mobility limited by scattering from the dislocation lines will be examined. Specifically, in the present work, the dependence of the electron drift and Hall mobilities on the threading dislocation line density, and the amount of charge accumulated along the threading dislocation lines within GaN and InN, will be computed separately.

This chapter is organized in the following manner. In Section 3.2, the formulation corresponding to the scattering of electrons from the dislocation lines within semiconductors will be presented. Results for the electron drift and Hall mobilities, limited by scattering from the threading dislocation lines within GaN and InN, are then presented in Sections 3.3 and 3.4, respectively.

3.2 Formulation

The formulation presented in this section follows closely the formulation developed in a paper by You *et al.* [60]. Similar to the other scattering mechanisms present within semiconductors, scattering from the dislocation lines should be treated quantum mechanically. In Figure 3.1(a), a representative scattering event from a dislocation line is depicted. In this figure, it is assumed that an electron, of a plane wave functional dependence, i.e., $\psi(\vec{k},\vec{r}) = \frac{1}{\sqrt{V}}\exp(i\vec{k}\cdot\vec{r})$, is incident upon the dislocation line and is scattered in a direction indicated by the wave vector, $\vec{k}'$. The incident and the scattered wave vectors, i.e., $\vec{k}$ and $\vec{k}'$, can be decomposed into components parallel and perpendicular to the dislocation line direction. The component parallel to the dislocation line direction, denoted by $\vec{k}_{\|}$ and $\vec{k}'_{\|}$, will not change during the scattering process, i.e., $\vec{k}_{\|} = \vec{k}'_{\|}$. For the perpendicular components of

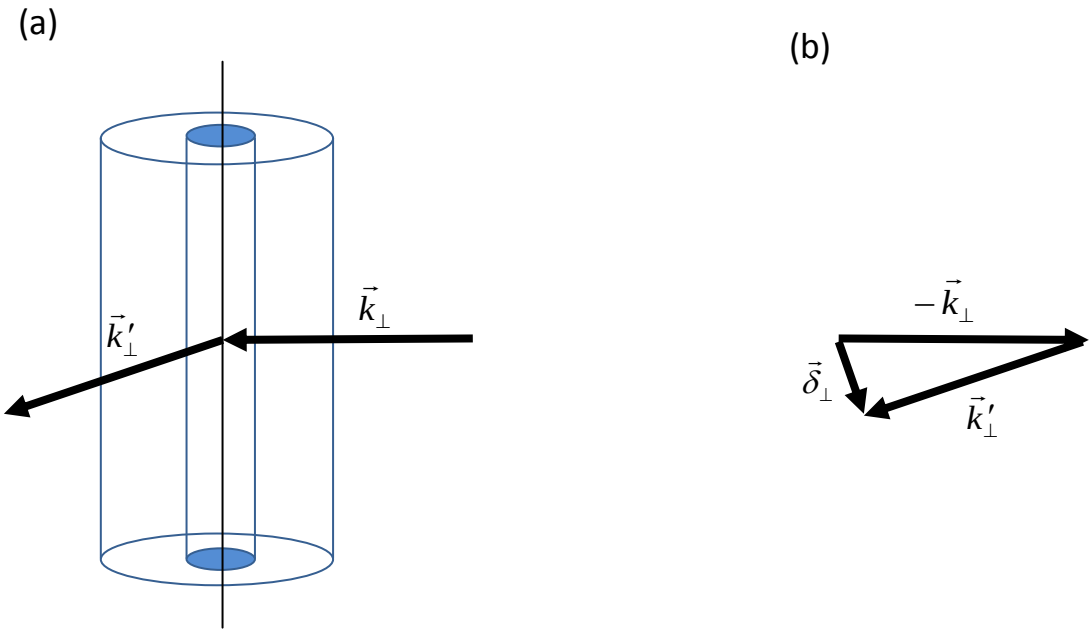

Figure 3.1: (a) Scattering of a plane wave with a wave vector $\vec{k}_\perp$, from a cylindrically symmetric potential, and (b) defining the wave vector difference, $\vec{\delta}_\perp$.

the incident and scattered wave vectors, $k_\perp = k'_\perp$, i.e., elastic scattering will be assumed.

In the Dirac bracket notation, the matrix element of the scattering potential in the incident and scattered wave functions may be expressed as

$$M(\delta_\perp) = \langle \psi(\vec{k}, \vec{r}) \, |\varphi(\vec{r})| \, \psi(\vec{k'}, \vec{r}) \rangle, \tag{3.7}$$

where $\delta_\perp$ is the magnitude of the wave vector difference, $\vec{\delta}_\perp$; see Figure 3.1(b). The Dirac bracket notation can be expanded in terms of the associated integral over the volume of the semiconductor material, V, to give

$$M(\delta_\perp) = \frac{1}{V} \int_V \exp(i\vec{\delta} \cdot \vec{r}) \varphi(\vec{r}) \, \mathrm{d}^3\vec{r}. \tag{3.8}$$

Since the scattering potential, $\varphi(\vec{r})$, has a solely radial dependence in cylindrical coordinates, this integration in cylindrical coordinates may be simplified, leading to

$$M(\delta_\perp) = \frac{1}{V} \int_0^H \int_0^{2\pi} \int_0^R \exp(i\delta_\perp r \cos(\phi)) \varphi(r) r \, \mathrm{d}z \, \mathrm{d}\phi \, \mathrm{d}r. \tag{3.9}$$

Performing the integrations over the z and ϕ coordinates of the cylindrical coordinate system, the matrix element may thus be expressed as

$$M(\delta_\perp) = \frac{2\pi}{S} \int_0^R J_0(\delta_\perp r) \varphi(r) r \, \mathrm{d}r, \tag{3.10}$$

where S is the surface area of the semiconductor material and $J_0(\delta_\perp r)$ denotes a Bessel function of the first kind of order 0, evaluated at $\delta_\perp r$. Ideally, the

integration in Eq. (3.10) should be computed for the radius, R, approaching infinity. In practice, however, since it is assumed that $\varphi(r) = 0$ for $r > R_{\mathrm{sc}}$, one need only take the radius, R, to be equal to R_{sc}.

In quantum physics, Fermi's golden rule is the way to calculate the transition rate (probability of transition per unit time) from one energy eigenstate of a quantum system into a continuum of energy eigenstates, due to a perturbation. According to Fermi's golden rule, the probability of the incident electron being scattered in the direction denoted by the wave vector, $\vec{k}'_{\perp}$, is proportional to the square modulus of the scattering matrix element, i.e., $|M(\delta_{\perp})|^2$. The scattering rate is thus given by

$$W(\vec{k}, \vec{k'}) = \frac{2\pi}{\hbar}|M(\delta_{\perp})|^2\delta(E_k - E_{k'}), \tag{3.11}$$

where the δ in the $\delta(E_k - E_{k'})$ term on the right hand side of Eq. (3.11), denotes the Dirac delta function, not to be confused with the $\delta_{\perp}$ defined earlier as the difference between the incident and scattered wave vectors in the perpendicular direction.

The average time that it takes for an electron to be successively scattered between the dislocation lines depends on the energy of the electron. For an electron characterized by a plane wave with a wave vector, $\vec{k}$, the kinetic

energy of the electron can be written as

$$E(k) = \frac{p^2}{2m_e^*}. \tag{3.12}$$

Substituting for the electron crystal momentum, $p = \hbar k$, into Eq. (3.12), the energy of the electron becomes related to its wave vector through the following relation

$$E(k) = \frac{\hbar^2 k^2}{2m_e^*}. \tag{3.13}$$

It can be shown that the relaxation time for the elastic scattering of an electron with incident wave vector, $\vec{k}$, is related to the scattering rate $W(\vec{k}, \vec{k'})$, through the following relationship [74]

$$\frac{1}{\tau(k)} = \int W(\vec{k}, \vec{k'}) \left[1 - \frac{\vec{v}_{\vec{k'}} \cdot \vec{\mathcal{E}}}{\vec{v}_{\vec{k}} \cdot \vec{\mathcal{E}}}\right] \frac{\mathrm{d}^3 k'}{(2\pi)^3}, \tag{3.14}$$

where $\vec{v}_{\vec{k}}$ and $\vec{v}_{\vec{k'}}$ denote the incident and the scattered electron velocities, respectively. As a result, in the present case of scattering from a cylindrical potential function, and for an electric field, $\vec{\mathcal{E}}$, applied in a direction perpendicular to the direction in which the threading dislocation lines extend, the relaxation time from one scatterer in a volume V, will be given by the following relationship

$$\frac{1}{\tau_{\mathrm{dis}}(k)} = \frac{m_e^*}{2\pi\hbar^3 k^3} \int_0^{2k} |M(\delta_\perp)|^2 \frac{{\delta_\perp}^2}{\sqrt{1 - (\delta_\perp/2k)^2}} \, \mathrm{d}\delta_\perp. \tag{3.15}$$

In Eq. (3.16), the integration runs over all possible values of the wave vector difference, $\delta_\perp$, i.e., it runs from the lower limit, 0, corresponding to negligible

scattering, to the higher limit, $2k$, corresponding to the complete backward scattering of the incident plane wave.

If the density of the threading dislocation lines is $\sigma_{\rm dis}$, then there are $\sigma_{\rm dis}S$ scatterers in the volume. It will be assumed that these dislocation lines are randomly placed and are well separated from each other so that the scattering is incoherent. In this case, according to quantum mechanics, one can simply sum the scattering rate from each scatterer. The total relaxation time is thus

$$\frac{1}{\tau_{\rm dis}(k)} = \frac{\sigma_{\rm dis} m_e^*}{2\pi\hbar^3 k^3} \int_0^{2k} \left|\tilde{M}(\delta_\perp)\right|^2 \frac{{\delta_\perp}^2}{\sqrt{1-(\delta_\perp/2k)^2}}\,{\rm d}\delta_\perp, \tag{3.16}$$

where $\tilde{M}(\delta_\perp) \equiv SM(\delta_\perp)$. The energy selective mean free time, $\tau_{\rm dis}(E)$, has to be integrated over all the energies of the incident wave vector in order to obtain the energy averaged mean free time, i.e.,

$$\langle\tau_{\rm dis}\rangle = \frac{4}{3\pi^{(1/2)}(k_BT)^{5/2}} \int_0^\infty \tau_{\rm dis}(E) E^{3/2} \exp(-E/k_BT)\,{\rm d}E. \tag{3.17}$$

In Eq. (3.17), the term $E^{3/2}\exp(-E/k_BT)$ in the integrand corresponds to the distribution of energies of the electrons within a semiconductor, which essentially acts as a weighting factor for the integration.

Similarly, the mean free time squared energy averaged, can be obtained from the following relationship [60]

$$\left\langle\tau_{\rm dis}^2\right\rangle = \frac{4}{3\pi^{(1/2)}(k_BT)^{5/2}} \int_0^\infty \tau_{\rm dis}^2(E) E^{3/2} \exp(-E/k_BT)\,{\rm d}E. \tag{3.18}$$

Finally, substitution of the expressions for $\langle \tau_{\text{dis}} \rangle$ and $\langle \tau_{\text{dis}}^2 \rangle$, from Eqs. (3.17) and (3.18), into Eqs. (3.3) and (3.4), gives the associated dislocation scattering limited electron drift and Hall mobilities, respectively.

3.3 Electron mobility limited by scattering from the charged threading dislocation lines within GaN

Substituting the electrostatic potential profiles obtained earlier in Figure 2.5 for $\varphi(r)$, in the formulation developed in Section 3.2, the electron drift and Hall mobilities within GaN can be computed numerically. The resultant dislocation limited electron drift and Hall mobilities are plotted as a function of the value of the negative charge accumulated along the dislocation lines, f, in Figures 3.2(a) and (b), respectively. The filled blue circles in these figures correspond to the result of these computations. The same GaN material parameters from Table 1.1, used earlier in obtaining the electrostatic potentials of Figure 2.5, have also been utilized for the purposes of the electron mobility computations in this section. Furthermore, since the electrostatic potentials in Figure 2.5 were obtained at room temperature

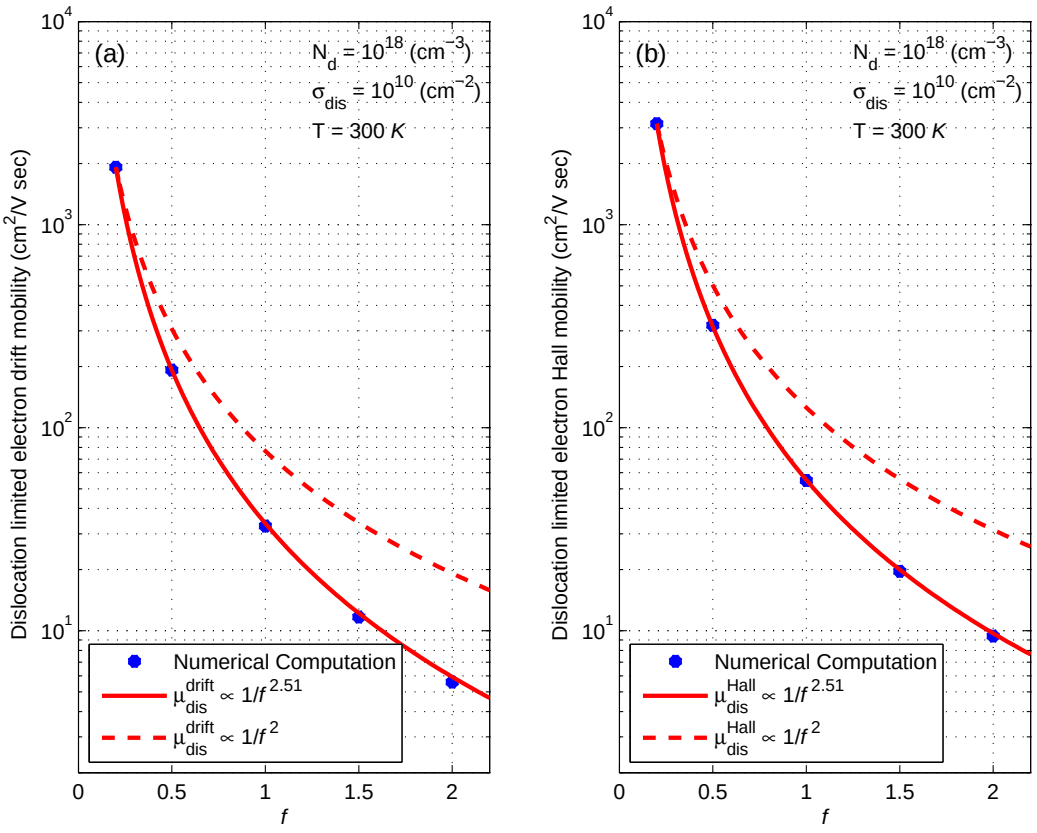

Figure 3.2: (a) The electron drift mobility and (b) the electron Hall mobility limited by scattering from charged threading dislocation lines within GaN.

and for a bulk donor concentration of $N_d = 10^{18}\,\mathrm{cm}^{-3}$, the same values of $T = 300$ K and $N_d = 10^{18}\,\mathrm{cm}^{-3}$ have also been assumed in the computation of the electron mobilities in this section. The electron mobilities presented in Figures 3.2(a) and (b) have been plotted for a dislocation line density of $\sigma_{\mathrm{dis}} = 10^{10}\,\mathrm{cm}^{-2}$. Since, within the formulation developed in Section 3.2, the electron mobilities are inversely proportional to the dislocation line density, σ_{dis} (recall Eq. (3.16)), deducing the values for the associated electron drift and Hall mobilities at other dislocation line densities, from the results depicted in Figures 3.2(a) and (b) would be straightforward.

If the electrostatic potentials depicted in Figure 2.5 were linearly proportional to the value of f, Eqs. (3.10) and (3.16) suggest that the computed electron drift and Hall mobilities would have a $1/f^2$ functional dependence. This $1/f^2$ functional dependence of the electron mobility is depicted with the dashed lines in Figures 3.2(a) and (b). However, from Figures 3.2(a) and (b), it is observed that a best fit to the computed electron mobility results is obtained for a $1/f^{2.51}$ functional dependence. Since the negative charge in the dislocation core cylinder scales linearly with the value of f, this overall dependence of the electron mobility on the value of f suggests that the bulk ionized donor screening occurring within GaN is less effective than a linear screening with increasing values of f.

3.4 Electron mobility limited by scattering from the charged threading dislocation lines within InN

In Figures 3.3(a) and (b), the dislocation limited electron drift and Hall mobilites are plotted as a function of the positive charge accumulated along the dislocation lines within InN, f. The electrostatic potentials obtained earlier in Figure 2.8, along with the InN material parameters given in Table 1.1, were used for the computation of these dislocation limited electron mobility results within InN. Since the electrostatic potentials in Figure 2.8 were obtained at room temperature and for a bulk donor concentration of $N_d = 10^{18}\,\mathrm{cm}^{-3}$, the same values of $T = 300$ K and $N_d = 10^{18}\,\mathrm{cm}^{-3}$ have also been assumed in the computation of the electron mobilities in this section. Furthermore, the electron mobilities depicted in Figures 3.3(a) and (b) have been plotted for a dislocation line density of $\sigma_{\mathrm{dis}} = 10^{10}\,\mathrm{cm}^{-2}$. Within the framework of the formulation of Section 2.2, utilized in obtaining the electron mobility results in this section, determining the dislocation limited electron mobilities for other threading dislocation line densities would be straightforward.

For the case of InN, from Figures 3.3(a) and (b) it is observed that a best

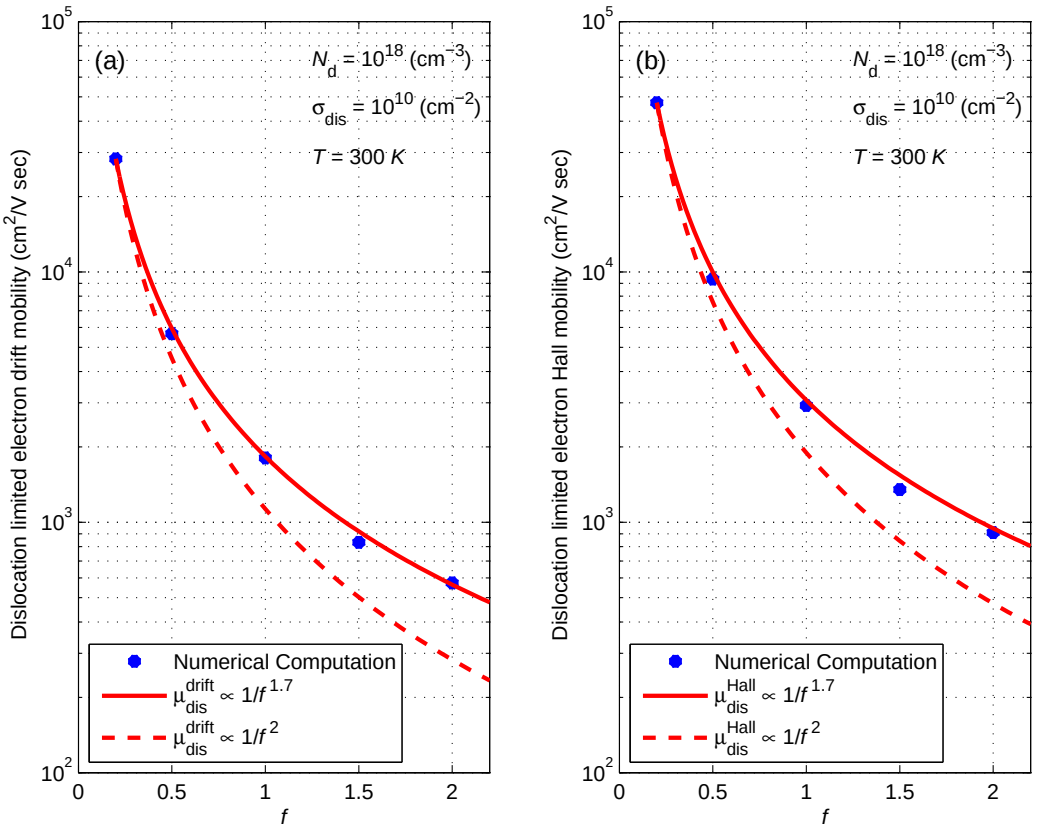

Figure 3.3: (a) The electron drift mobility and (b) the electron Hall mobility limited by scattering from charged threading dislocation lines within InN.

fit to the computed electron mobility results is obtained for a $1/f^{1.7}$ functional dependence. Since the positive charge in the dislocation core cylinder scales linearly with the value of f, this overall dependence of the electron mobilities on the value of f suggests that the predominantly free electron screening of the dislocation lines within InN is more effective than a linear screening with increasing values of f.

Furthermore, in terms of the absolute electron mobility values, under the same n-type bulk doping conditions, it is observed that the electron drift and Hall mobilities within InN are much higher than those computed for the case of GaN. This higher electron mobility within InN can be attributed to the much stronger screening of the dislocation core charge within InN as well as the lower value for the electron effective mass of InN.

Chapter 4

Occupation statistics of the dislocation defect sites

4.1 Different approaches for the determination of the dislocation defect site occupation statistics

In the previous two chapters, computations of the screening space charge distribution functions, the scattering potentials, and the electron mobilities, were reported for five different representative values of f, for the cases of both GaN and InN. In general, however, the value of f can be kept as a

variable of the formulation and determined as a function of the bulk donor concentration. In fact, determining the value of f as a function of the free carrier concentration and/or bulk doping concentration within n-type GaN has been the subject of several studies in the literature [39, 60, 75, 76, 77].

In this chapter, theoretical means of determining the value of f from knowledge of the free carrier concentration and/or the bulk doping concentration within GaN and InN is developed. Initially, a survey of theoretical formulations that are available in the literature is provided. Later, a simple Gibbs factor formalism will be introduced, which allows for a determination of the occupation statistics of multiple ionization states associated with a dislocation defect site. Thus far, the treatment of multiple ionization states associated with a dislocation defect site has only been achieved in the literature through the use of either detailed numerical density functional calculations [76] or through tedious energy minimization computations [60, 77]. The formulation provided herein, represents a break from this tradition, allowing for the presentation of intuitively appealing results.

Understanding the occupation statistics of the defect sites associated with the dislocation lines within semiconductor materials has been the focus of much attention over the years. The model of Read [73], developed in 1954, remains the dominant approach used for the characterization of the occupa-

tion of the defect sites associated with the threading dislocation lines within semiconductor materials. The model of Read [73] pictures a dislocation line within the crystal structure (as was initially applied to germanium) as being comprised of a column of identical and equally spaced dangling bonds, as was shown in Figure 1.5. Each dangling bond can potentially trap an extra electron from a nearby donor atom. The model of Read [73] assumes that the screening of the charge trapped by the dangling bonds along a dislocation line is provided for by the complete ionization of the bulk donor atoms in the immediate vicinity of the dislocation line, up to a certain radius, referred to as the Read radius, R. The Read radius can be readily obtained in terms of the charge trapped along the dislocation lines per dislocation defect site, f, and the bulk donor concentration, N_d, i.e.,

$$R = \sqrt{\frac{f}{\pi c N_d}}. \tag{4.1}$$

As some of the dangling bonds trap an extra electron, an electrostatic potential begins to build up, preventing the remaining dangling bonds from becoming negatively charged. Read [73] determined the fraction, f, of dangling bonds that would actually trap electrons by minimizing the electrostatic energy within the space charge region formed about each dislocation line.

In 1998, Weimann *et al.* [39] employed the model of Read [73] as the basis for obtaining the occupation statistics of the defect sites associated with the

threading dislocation lines within GaN. For the purposes of their computations, Weimann *et al.* [39] assumed a simple dangling bond model for the dislocation core structure. Gurusinghe and Andersson [75] also followed the general approach presented by Read [73]. However, instead of minimizing the electrostatic potential energy within the space charge cylinder, they minimized the corresponding Helmholtz free energy. You *et al.* [60] also followed the energy minimization approach of Read [73]. However, instead of picturing each dislocation line as a simple column of dangling bonds, they assumed a realistic $V_{Ga} - O_N$ core structure for the threading dislocation lines. Leung *et al.* [76] obtained the occupation statistics of the threading dislocation lines within GaN for a number of different dislocation core structures, for both p-type and n-type doping conditions. Leung *et al.* [76] used a simulated annealing approach, which is essentially a numerical density functional calculation. Results obtained through the application of the proposed Gibbs factor formulation presented in this thesis to the problem of determining the occupation statistics of threading dislocation lines within GaN will be compared with these other approaches in this chapter.

This chapter is organized in the following manner. In Section 4.2, the general Gibbs factor formalism, and its formulation within semiconductor materials, will be presented. In Section 4.3, the electrostatic potential at the

site of a dislocation defect, resulting from the charge on the other dislocation defect sites along the dislocation line, will be obtained. In Section 4.4, simple analytical expressions will be proposed to approximate the actual screening space charge distributions of the dislocation lines within GaN and InN, separately. In Section 4.5, the proposed Gibbs factor formalism will be applied to the specific case of dislocation lines within GaN with an assumed dangling bond dislocation core structure. In Section 4.6, the Gibbs factor formalism will be applied to the problem of determining the occupation statistics of the $V_{Ga} - O_N$ dislocation defect sites within GaN. In Section 4.7, a 5/7-ring core structure will be assumed for the determination of the occupation statistics of the dislocation defect sites within wurtzite InN.

4.2 Gibbs factor formalism

The probability of a quantum mechanical system, in thermal and diffusive equilibrium with a reservoir, to exist in each of its different ionization states is proportional to the corresponding Gibbs factor of the system in that particular state. The absolute probability that the system will be found in a state with N_1 electrons, with an associated total energy of ε_1, is given by the Gibbs factor associated with that state, divided by the grand partition

function, i.e.,

$$P(N_1, \varepsilon_1) = \frac{\exp\left[\left(N_1\mu - \varepsilon_1\right)/k_B T\right]}{Z}, \tag{4.2}$$

where μ denotes the chemical potential of the system/reservoir. The grand partition function, Z, is simply the summation of the Gibbs factors associated with the different possible states of the quantum mechanical system, i.e.,

$$Z(\varepsilon_{\mathrm{F}}, T) = \sum_{N_e=0}^{\infty} \sum_{s(N_e)} \exp\left[\left(N_e\mu - \varepsilon_{s(N_e)}\right)/k_B T\right]. \tag{4.3}$$

In Eq. (4.3), the first summation runs over the number of electrons within the quantum mechanical system. Even though in Eq. (4.3) this summation runs from zero to infinity, in practice, only a few ionization states of the system are most probable and thus, to a good approximation, this summation need only be run over two or three electrons. The second summation, i.e., the summation over $s(N_e)$, is a summation that runs over all the different possible quantum mechanical states of the system when it consists of N_e electrons.

In the context of semiconductor physics, the chemical potential associated with the electrons, μ, is referred to as the Fermi energy level, ε_{F}. Furthermore, for the case of the dislocation lines within semiconductors, each dislocation defect site serves the purpose of the quantum mechanical system, and the bulk of the semiconductor material serves the purpose of the reservoir with which the dislocation defect site should remain in thermal and

diffusive equilibrium. In general, it is possible that for some dislocation core structures, the associated defect sites introduce a multitude of energy levels into the energy band structure of the semiconductor material. For example, in Figure 4.1, the multitude of energy levels that the full core, the open core, the gallium vacancy, and the nitrogen vacancy dislocation core structures introduce into the energy band of GaN are depicted. However, under any given bulk doping condition, most of those energy levels remain either completely occupied or completely unoccupied, and thus, need not be included in the evaluation of the grand partition function. As a result, in this thesis, it will be assumed that each dislocation defect site introduces a single energy level, ε_t, into the energy gap of the semiconductor. This energy level can exist in any of the four different occupation states depicted in Figure 4.2.

According to the Gibbs factor formalism, the probability of the dislocation defect site to exist in each of these states is given by

$$f_{s(0)} = \frac{1}{Z}, \tag{4.4}$$

$$f_{s(1\uparrow)} = f_{s(1\downarrow)} = \frac{f_{s(1)}}{2} = \frac{\exp\left[\left(\varepsilon_{s(1)} - \varepsilon_{\mathrm{F}}\right)/k_B T\right]}{Z}, \tag{4.5}$$

$$f_{s(2)} = \frac{\exp\left[\left(\varepsilon_{s(2)} - 2\varepsilon_{\mathrm{F}}\right)/k_B T\right]}{Z}, \tag{4.6}$$

with

$$Z = 1 + 2\exp\left[\left(\varepsilon_{s(1)} - \varepsilon_{\mathrm{F}}\right)/k_B T\right] + \exp\left[\left(\varepsilon_{s(2)} - 2\varepsilon_{\mathrm{F}}\right)/k_B T\right], \tag{4.7}$$

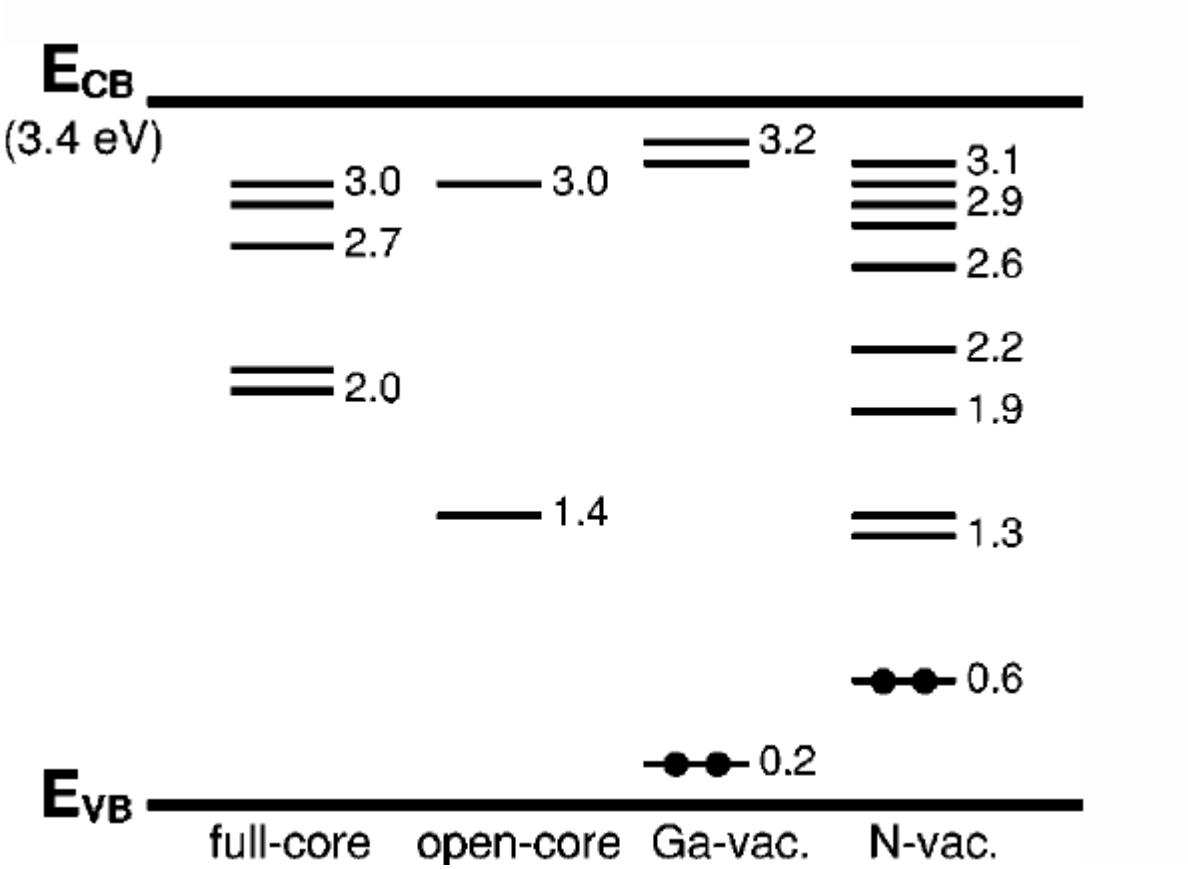

Figure 4.1: The schematic diagram of energy levels in the band gap for four different dislocation core structures within GaN. This figure is after Lee *et al.* [57].

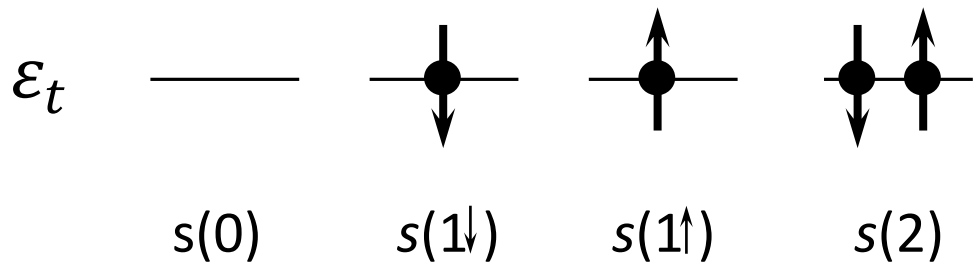

Figure 4.2: The four possible occupation states of a dislocation defect site.

$\varepsilon_{s(1)}$ and $\varepsilon_{s(2)}$ representing the total energy of the dislocation defect site in the states labelled by $s(1)$ and $s(2)$ in Figure 4.2, respectively.

In order to relate the energies $\varepsilon_{s(1)}$ and $\varepsilon_{s(2)}$ to the dislocation defect energy level, ε_t, it is recalled, from Section 2.2, that the effect of the electrostatic potential, $\varphi(r)$, in the neighbourhood of the dislocation core is to shift all of the electronic energy levels by the amount $-q\varphi(r)$ relative to the Fermi energy level, ε_{F}. For the single electron occupancy of a dislocation defect site, i.e., in either of the $s(1\uparrow)$ or $s(1\downarrow)$ states, the energy of the single electron residing in the dislocation defect site will thus be shifted by the value of the electrostatic potential at the site of the dislocation defect, φ_0, multiplied by the charge of the electron, i.e.,

$$\varepsilon_{s(1)} = \varepsilon_t - q\varphi_0. \tag{4.8}$$

If the electron-electron repulsion of the two electrons in the state $s(2)$ is neglected, the energy of the double occupancy of the dislocation defect site will simply be twice that of the single occupancy of the dislocation defect site, i.e.,

$$\varepsilon_{s(2)} = 2 \times \varepsilon_{s(1)}. \tag{4.9}$$

In general, however, this electron-electron repulsion causes the dislocation defect energy level, ε_t, to split into two energies, $\varepsilon_t^{(1)}$ and $\varepsilon_t^{(2)}$, much like

the first and second ionization energies of a helium atom. In the case of a dislocation defect site in the presence of inner electron-electron interactions, $\varepsilon_t^{(1)}$ will be the energy of the single electron in either of the states $s(1\uparrow)$ or $s(1\downarrow)$. Due to the electrostatic repulsion from the first existing electron in the state $s(2)$, the energy of the second electron in the state $s(2)$, $\varepsilon_t^{(2)}$, will be higher than that of the single electron in the state $s(1)$, i.e., $\varepsilon_t^{(2)} > \varepsilon_t^{(1)}$. In the presence of electron-electron repulsions within each dislocation defect site, the total energies of the defect site in its different occupation states should thus be written as

$$\varepsilon_{s(1)} = \varepsilon_t^{(1)} - q\varphi_0, \tag{4.10}$$

and

$$\varepsilon_{s(2)} = \varepsilon_{s(1)} + \left(\varepsilon_t^{(2)} - q\varphi_0\right). \tag{4.11}$$

The value of the electrostatic potential at the site of a dislocation defect, φ_o, is due to the presence of (1) the charge accumulated on the other defect sites situated along the dislocation line, and (2) the screening space charge distribution. The contribution from these two charge build-ups will henceforth be denoted by $\varphi_{o_{\rm dc}}$ and $\varphi_{o_{\rm sc}}$, respectively. As a result, the electrostatic potential at the site of a dislocation defect can be expressed as

$$\varphi_o = \varphi_{o_{\rm dc}} + \varphi_{o_{\rm sc}}. \tag{4.12}$$

Taking the discreteness of the charge residing on the dislocation defect sites into account, in the following section, an approximate expression for $\varphi_{o_{\rm dc}}$ will be derived. Then, in Section 4.4, simple analytical expressions will be obtained for the electrostatic potential, $\varphi_{o_{\rm sc}}$, by virtue of approximating the actual screening space charge distributions, obtained earlier in Figures 2.4 and 2.7, by some alternative simple analytical functions.

4.3 Approximating the electrostatic potential induced by the dislocation core charge

In this section, the aim is to obtain an approximate analytical expression for the electrostatic potential, $\varphi_{o_{\rm dc}}$. Specifically, the discreteness of the charge on the defect sites along the dislocation line will be taken into account and the dislocation line will be assumed to have a finite height, h. Assuming the distance between the successive dislocation defect sites to be equal to the c-lattice constant associated with the wurtzite crystal structure of GaN/InN, a total of h/c defect sites exist on the dislocation line. Consequently, the number of defect sites residing in the four dislocation defect occupation states $s(0)$, $s(1\downarrow)$, $s(1\uparrow)$, and $s(2)$, can be obtained from the following relations

$$N_{s(0)} = \frac{h f_{s(0)}}{c}, \tag{4.13}$$

$$N_{s(1\downarrow)} = N_{s(1\uparrow)} = \frac{N_{s(1)}}{2} = \frac{hf_{s(1\downarrow)}}{c} = \frac{hf_{s(1\uparrow)}}{c} = \frac{hf_{s(1)}}{2c}, \tag{4.14}$$

and

$$N_{s(2)} = \frac{hf_{s(2)}}{c}, \tag{4.15}$$

respectively. Furthermore, it will be assumed that, in units of the fundamental electron charge, the dislocation defect site in each of the four states $s(0)$, $s(1\downarrow)$, $s(1\uparrow)$, and $s(2)$, has a net charge of $i_{s(0)}$, $i_{s(1\downarrow)}$, $i_{s(1\uparrow)}$, and $i_{s(2)}$ associated with it. The average charge per dislocation defect site, in units of the fundamental electron charge, can thus be obtained from the following relation

$$f = \left| i_{s(0)} \times N_{s(0)} + 2 \times i_{s(1\downarrow)} \times N_{s(1\downarrow)} + i_{s(2)} \times N_{s(2)} \right|. \tag{4.16}$$

Recall that in Chapters 2 and 3, five different representative values for the average charge per dislocation defect site, f, were considered, i.e., 0.2, 0.5, 1, 1.5, and 2. In the context of the Gibbs factor formalism developed in this chapter, however, from Eq. (4.16) and Eqs. (4.4) to (4.6), it is now seen how the average charge per dislocation defect site, f, can be related to the value of the electrostatic potential at the site of a dislocation defect.

For a dislocation defect site situated in the middle of a dislocation line of height, h, one half of the other dislocation defect sites lie above this defect site and one half lie below this dislocation defect site. As a result, taking the

discreteness of the charge on the other dislocation defect sites into account, the electrostatic potential due to the other defect sites along the dislocation line, at the site of a defect in the middle of the dislocation line, can be expressed as

$$\varphi_{o_{\mathrm{dc}}} = 2\frac{\varepsilon_0 f_{s(0)} i_{s(0)}}{q} \sum_{n=1}^{N_{s(0)}/2} \frac{1}{n} + 2\frac{\varepsilon_0 f_{s(1)} i_{s(1)}}{q} \sum_{n=1}^{N_{s(1)}/2} \frac{1}{n} + 2\frac{\varepsilon_0 f_{s(2)} i_{s(2)}}{q} \sum_{n=1}^{N_{s(2)}/2} \frac{1}{n}, \tag{4.17}$$

where

$$\varepsilon_0 \equiv \frac{q^2}{4\pi\epsilon_r\epsilon_o c}. \tag{4.18}$$

In order to express the result of the summation, $\sum_{n=1}^{N} \frac{1}{n}$, in a closed analytical form, Read [73] employed the approximation, $\sum_{n=1}^{N} \frac{1}{n} \approx \ln(N) + 0.577$, which is valid for large values of N. In the present thesis, however, in order to make a corresponding approximation, which will be valid for small values of N as well, the following series expansion approximation will be made

$$\sum_{n=1}^{N} \frac{1}{n} \approx \ln(N+1) + 0.577, \tag{4.19}$$

where the value, 0.577, is an approximation to Euler's constant. In Figure 4.3, the value of the two expressions on the left and right hand side of Eq. (4.19) have been plotted as a function of N, with the red and blue curves, respectively.

Substituting the approximate expression for $\sum_{n=1}^{N} \frac{1}{n}$, i.e., Eq. (4.19), into

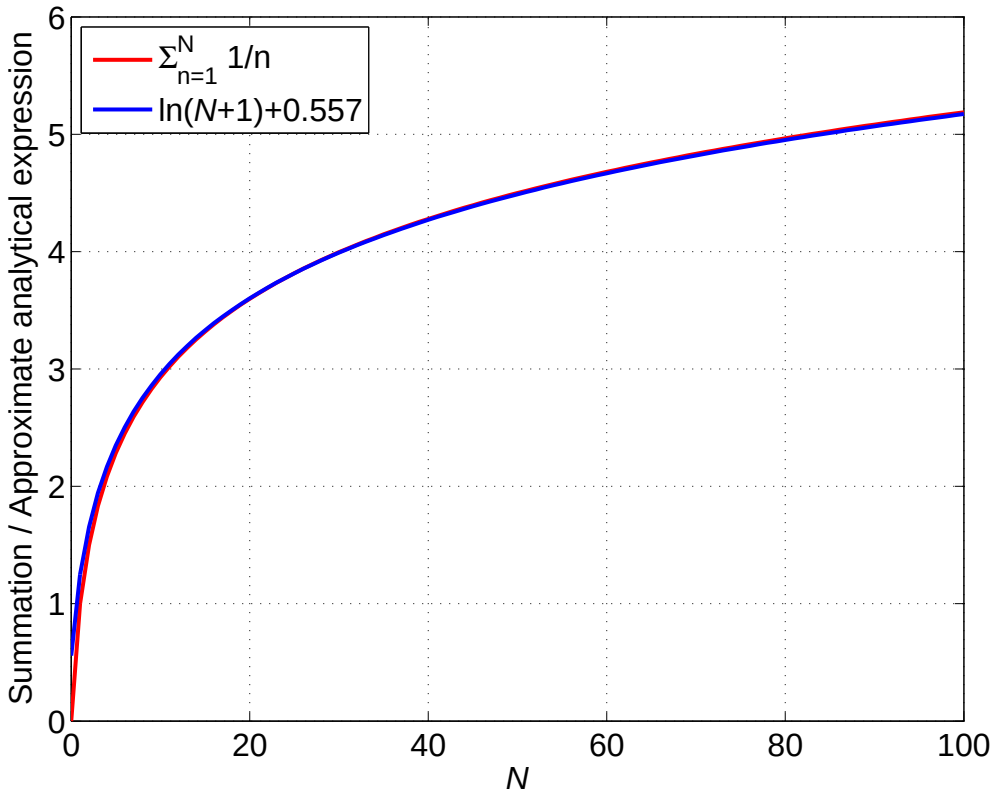

Figure 4.3: Comparison of the exact and the suggested approximation to the value of the summation, $\sum_{n=1}^{N} \frac{1}{n}$, as a function of N.

Eq. (4.17), the electrostatic potential, $\varphi_{o_{\rm dc}}$, can thus be finally written as

$$\varphi_{o_{\rm dc}} = 2\frac{\varepsilon_0}{q}\left\{f_{s(0)}i_{s(0)}\left(\ln\left(N_{s(0)}/2+1\right)+0.577\right)+\right.$$
$$f_{s(1)}i_{s(1)}\left(\ln\left(N_{s(1)}/2+1\right)+0.577\right)+$$
$$\left.f_{s(2)}i_{s(2)}\left(\ln\left(N_{s(2)}/2+1\right)+0.577\right)\right\}. \qquad (4.20)$$

4.4 Approximating the screening space charge distribution function

In general, one would like to take the value of the charge per dislocation defect site, f, as a variable, in addition to the two existing variables, $n_{\rm s}(r)$ and $\varphi(r)$, and solve simultaneously for the three variables. However, simple analytical expressions can only be obtained for the value of the electrostatic potential, if the screening space charge distribution function, $n_{\rm sc}(r)$, is approximated with a simple analytical functional form.

In the case of the predominantly ionized bulk donor screening, the screening space charge distribution function may be approximated by a step function. In Figure 4.4, both the exact and the suggested approximation to the screening space charge distribution functions have been depicted for the representative case of GaN. The red curve in Figure 4.4 is identical to the exact

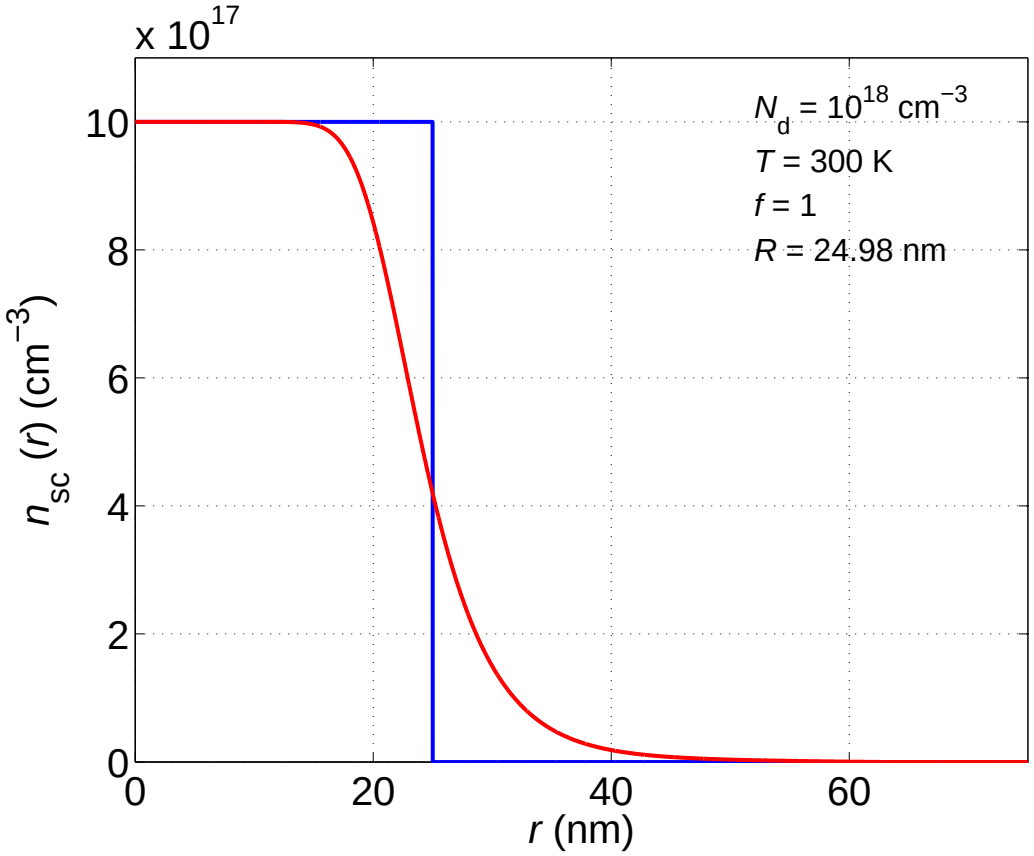

Figure 4.4: The approximation of the screening space charge distribution function surrounding a threading dislocation line within GaN by a step function.

screening space charge distribution result for the value of $f = 1$, obtained earlier in Figure 2.4. In the suggested approximate screening space charge distribution function depicted by the blue curve in Figure 4.4, the radius at which the screening space charge distribution drops off to zero, has been set to the Read radius, R, i.e., it is assumed that

$$n_{\rm sc}(r) \approx \begin{cases} N_{\rm d}, & r \leq R \\ 0, & r > R \end{cases} . \tag{4.21}$$

When determining the radial functional form of the electrostatic potential resulting from such a step function space charge distribution, Read [73] assumed the corresponding space charge cylinder to be of a finite height, h, and determined the corresponding electrostatic potential function, at midpoint along the height of the cylinder to be

$$\varphi_{\rm sc}(r) = f\frac{\varepsilon_0}{q}\left\{1 + 2\ln\left(\frac{h}{R}\right) - \frac{r^2}{R^2}\right\}, \tag{4.22}$$

where f refers to the average negative charge per dislocation defect site. Thus, at the site of a dislocation defect, i.e., at a radial distance $r = 0$ from the dislocation line

$$\varphi_{o_{\rm sc}} = f\frac{\varepsilon_0}{q}\left\{1 + 2\ln\left(\frac{h}{R}\right)\right\}. \tag{4.23}$$

For the case of InN, the predominantly free electron screening will be approximated by an exponential function, i.e.,

$$n_{\rm sc}(r) \approx n_0 \exp(-r/\lambda). \tag{4.24}$$

The parameter n_0 in Eq. (4.24) can be obtained through the requirement that the total negative charge subtended by the exponential function equals the positive charge of f per dislocation defect site along the dislocation line, i.e.,

$$n_0 = 2f\frac{\varepsilon_0}{q\lambda^2}. \tag{4.25}$$

In Figure 4.5, both the exact and the suggested approximation to the screening space charge distribution functions have been depicted for the representative case of InN. The red curve in Figure 4.5 is identical to the exact screening space charge distribution result for the value of $f = 1$, obtained earlier in Figure 2.7. It is observed that a best exponential functional fit to the exact screening space charge distribution in Figure 4.5 is obtained for λ being set to 2.6 nm.

In the case of an exponential screening space charge distribution function, the resultant radial functional form for the electrostatic potential, midpoint along a cylinder of height, h, can be obtained as

$$\varphi_{\rm sc}(r) = 2f\frac{\varepsilon_0}{q}\left\{\exp\left(-r/\lambda\right) + \int_0^{r/\lambda}\frac{1-\exp(-\xi)}{\xi}\,{\rm d}\xi + \ln\left(\frac{\lambda}{h}\right) - 0.577\right\}, \tag{4.26}$$

where ε_0 is the same as that defined earlier, i.e., in Eq. (4.18). The value of the electrostatic potential resulting from the exponential charge distribution at the site of a dislocation defect, i.e., at radial distance $r = 0$ from the

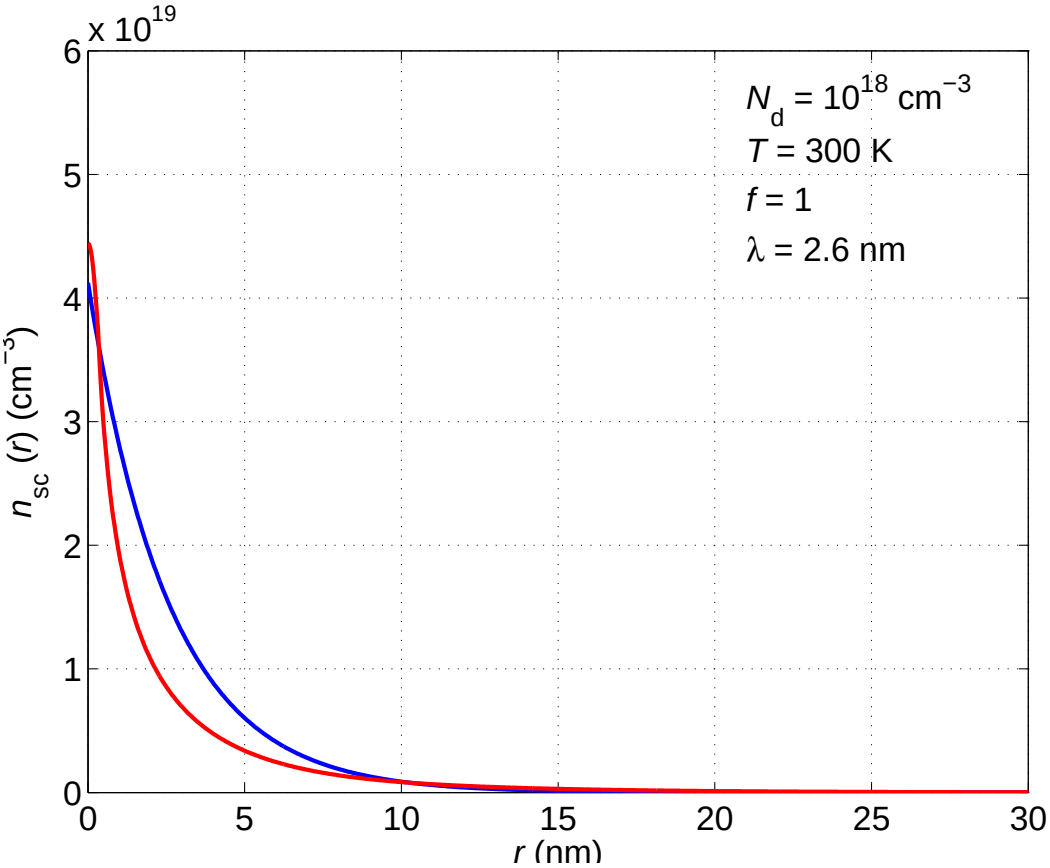

Figure 4.5: The approximation of the screening space charge surrounding a dislocation line within InN by an exponential function.

dislocation line, can be readily obtained from Eq. (4.26), i.e.,

$$\varphi_{o_{\rm sc}} = 2f\frac{\varepsilon_0}{q}\left\{1 - 0.577 + \ln\left(\frac{\lambda}{h}\right)\right\}. \tag{4.27}$$

In Sections 4.5 and 4.6, the expression obtained for $\varphi_{o_{\rm sc}}$ in Eq. (4.23) will be used in order to obtain the occupation statistics of the threading dislocation lines within n-type GaN for two different dislocation core structures. In Section 4.7, the expression obtained for $\varphi_{o_{\rm sc}}$ in Eq. (4.27) will be used in order to obtain the occupation statistics of the threading dislocation lines within n-type InN.

4.5 Occupation statistics of the dangling bond dislocation core structure within GaN

In this section, the Gibbs factor formalism formulated in Section 4.2 will be applied to the problem of determining the occupation statistics of the dislocation lines within GaN. For the sake of comparison with results already published in the literature, the dislocation core structure, assumed for the computations in this section, will be the same picture of dislocations used by Weimann *et al.* [39], i.e., a column of identical and equally spaced dangling bonds, with the distance between the successive dangling bonds

being taken as the c-lattice constant, c, associated with wurtzite GaN. In this and the following section, in order to take the effect of the charge trapped by the defect sites along the threading dislocation lines on the free electron concentration of the entire semiconductor material into account, the following overall charge neatrality condition will be used

$$N_{\rm d} = n + f\frac{\sigma_{\rm dis}}{c}. \tag{4.28}$$

In writing Eq. (4.28), the bulk donor atoms have been assumed to be completely ionized, i.e., $N_{\rm d}^{+} = N_{\rm d}$. The term, n, on the right hand side of Eq. (4.28) is then the fraction of the electrons donated by the bulk donor atoms which exist as free electrons, whereas the term, $f\sigma_{\rm dis}/c$, will be the fraction of the electrons donated by the bulk donor atoms which have become trapped by the dislocation defect sites. Furthermore, the full degenerate relation,

$$n = N_c\frac{2}{\sqrt{\pi}}\int_0^{\infty}\frac{\sqrt{x}}{1+\exp\left[x-(\varepsilon_{\rm F}-\varepsilon_c)/kT\right]}\,{\rm d}x, \tag{4.29}$$

for the free electron concentration within a semiconductor material, can be used along with Eq. (4.28) in order to obtain the position of the Fermi energy level, $\varepsilon_{\rm F}$, for known values of $N_{\rm d}$ and $\sigma_{\rm dis}$.

For the dangling bond dislocation core structure, the neutral state of a dangling bond corresponds to either of the states, $s(1\downarrow)$ or $s(1\uparrow)$, i.e., $i_{s(1\downarrow)} =$

$i_{s(1\uparrow)} = 0$. As the dangling bond loses an electron, it becomes positively charged and thus $i_{s(0)} = +1$. On the other hand, as each dangling bond traps an extra electron, it becomes negatively charged and the occupation state, $s(2)$, corresponds to a state of charge $i_{s(2)} = -1$. For these ionization states, the value of the electrostatic potential, $\varphi_{o_{\rm dc}}$, can be obtained from Eq. (4.20) as follows

$$\varphi_{o_{\rm dc}} = 2\frac{\varepsilon_0}{q}\left\{f_{s(0)}\left[\ln\left(N_{s(0)}/2+1\right)+0.577\right] - f_{s(2)}\left[\ln\left(N_{s(2)}/2+1\right)+0.577\right]\right\}, \tag{4.30}$$

and, from Eq. (4.16), the average charge per dangling bond is given by

$$f = f_{s(2)} - f_{s(0)}. \tag{4.31}$$

The value of the electrostatic potential at the site of a dangling bond, due to the screening space charge of ionized bulk donor atoms, was obtained earlier in Section 4.4 as

$$\varphi_{o_{\rm sc}} = f\frac{\varepsilon_0}{q}\left\{1+2\ln\left(\frac{N_{s(2)}c/f_{s(2)}}{R}\right)\right\}, \tag{4.32}$$

where in this relation, the equivalent expression, $N_{s(2)}c/f_{s(2)}$, has been replaced for the height h in Eq. (4.23). Finally, substituting for $\varphi_{o_{\rm dc}}$ and $\varphi_{o_{\rm sc}}$, from Eqs. (4.30) and (4.32) into Eq. (4.12), the value of the electrostatic potential at the site of a dangling bond within wurtzite GaN, can be written

as

$$\varphi_o = 2\frac{\varepsilon_0}{q}\Bigg\{ f_{s(0)}\left[\ln\left(N_{s(0)}/2+1\right)+0.577\right] - f_{s(2)}\left[\ln\left(N_{s(2)}/2+1\right)+0.577\right] + \frac{f_{s(2)}-f_{s(0)}}{2}\left[1+2\ln\left(\frac{N_{s(2)}c/f_{s(2)}}{R}\right)\right]\Bigg\}. \tag{4.33}$$

The quantities, ε_0, R, $f_{s(0)}$, $f_{s(2)}$, and $N_{s(0)}$ in Eq. (4.33) were all given in terms of the material parameters and/or other quantities, earlier in Eqs. (4.18), (4.1), (4.4), (4.6), and (4.13), respectively. In particular, from Eqs. (4.4) and (4.6), it is seen that $f_{s(0)}$ and $f_{s(2)}$ are expressed in terms of the energies, $\varepsilon_{s(1)}$, $\varepsilon_{s(2)}$, and $\varepsilon_{\rm F}$. As was mentioned at the outset of this section, for given values of $\sigma_{\rm dis}$ and $N_{\rm d}$, $\varepsilon_{\rm F}$ can be obtained from Eq. (4.28). Furthermore, for the purposes of the computations in this section, the energies, $\varepsilon_{s(1)}$ and $\varepsilon_{s(2)}$, will be related to φ_o and ε_t, through the use of Eqs. (4.8) and (4.9), i.e., the inner-dangling bond electron-electron interactions will be ignored. The position of the dislocation defect energy level, ε_t, will be set to 1.2 eV above the valence band maximum, in agreement with the value adopted by Weimann *et al.* [39] and Gurusinghe and Andersson [75]. For concreteness, the value of $N_{s(2)}$ will be set to 10^5, i.e., long dislocation lines will be assumed; as long as the value of $N_{s(2)}$ is sufficiently large, its value will not affect the electrostatic potential, φ_o, obtained. Thus, for any specific value of the bulk donor

density, N_d, Eq. (4.33) can be solved for the single variable, φ_o, once all the necessary substitutions have been made from the other equations.

After the electrostatic potential, φ_o, has been solved for from Eq. (4.33), its value can be plugged into Eqs. (4.4) through (4.7) in order to obtain the occupation probabilities, $f_{s(0)}$, $f_{s(1)}$, and $f_{s(2)}$, associated with a dislocation dangling bond. In Figure 4.6, the fraction of the dislocation dangling bonds in their different possible $f_{s(0)}$, $f_{s(1)}$, and $f_{s(2)}$ occupation states have been plotted as a function of the bulk donor concentration; in order to emphasize the charge residing on the dangling bonds, in Figure 4.6 the occupation fractions, $f_{s(0)}$, $f_{s(1)}$, and $f_{s(2)}$, have alternatively been labelled as f_{+1}, f_0, and f_{-1}, respectively, these new subscripts representing the corresponding charge states. The material parameters used for these computations are as specified in Table 1.1. These calculations were performed at 300 K for a dislocation line density of 10^8 cm^{-2}. It is seen from this figure that, under bulk n-type doping conditions, most of the dislocation defect sites are negatively charged. However, at lower bulk donor concentrations, a non-negligible fraction of the dislocation defect sites also become positively charged.

Experimentally, it has been observed that the threading dislocation lines within GaN become positively charged under bulk p-type doping conditions [69]. The proposed Gibbs factor formalism allows for the dislocation

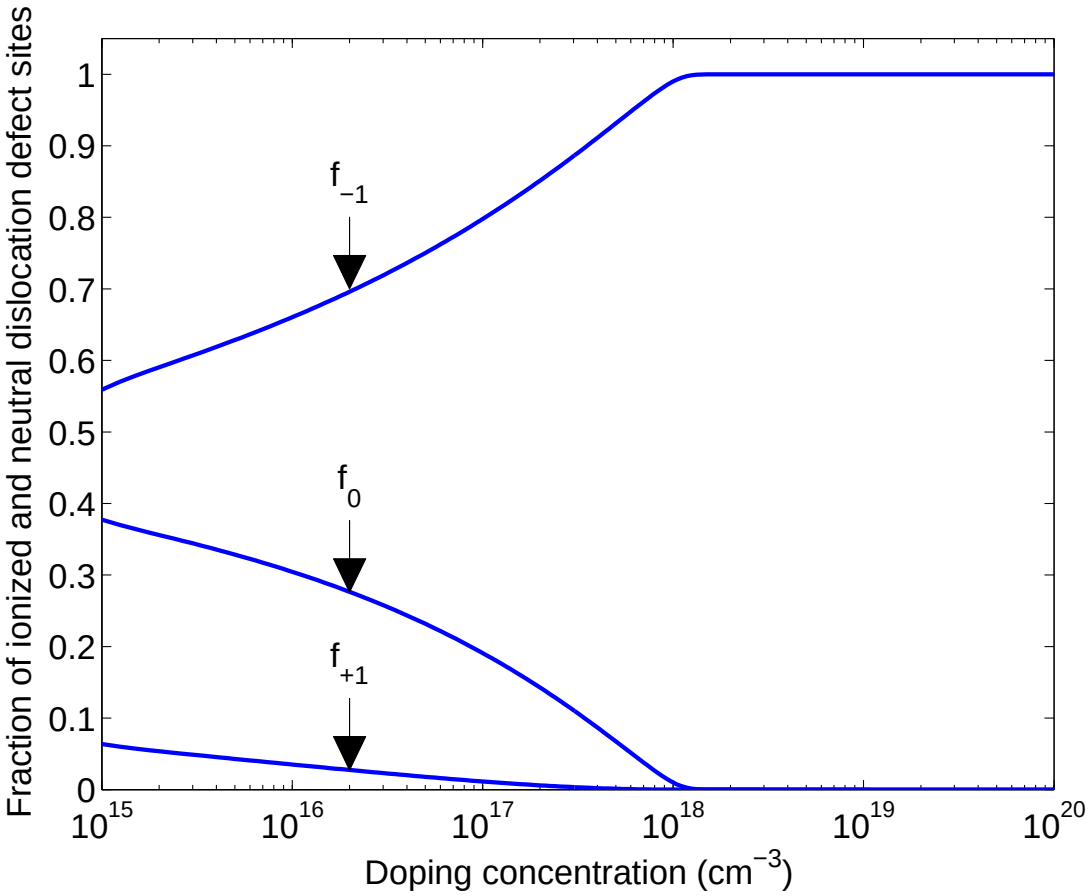

Figure 4.6: The fraction of ionized and neutral dislocation defect sites for a dangling bond core structure of the dislocation lines within n-type GaN as a function of the bulk donor concentration.

defect sites to be positively charged as well. As a result, the proposed Gibbs factor formalism can potentially be applied to p-type doping conditions as well.

In Figure 4.7, the average charge per dangling bond, f, is plotted as a function of the free electron concentration, n. Also plotted in this figure are the results from Weimann *et al.* [39] and from Gurusinghe and Andersson [75] for the same dislocation line density of $\sigma_{\text{dis}} = 10^8$ cm^{-2}. From Figure 4.7, it is observed that the results obtained from the application of the Gibbs factor formalism in this work [78], clearly favour the results of Gurusinghe and Andersson [75] over the results reported by Weimann *et al.* [39]. The considerable difference between the reproduced result of Weimann *et al.* [39] and the others depicted in Figure 4.7 are most likely a consequence of different parameter value selections; through a detailed critical comparative analysis, it is found that the results of Weimann *et al.* [39] may be exactly reproduced by selecting a dislocation energy level, ε_t, of 2.02 eV above the valence band edge, all other parameters being as set in Table I.

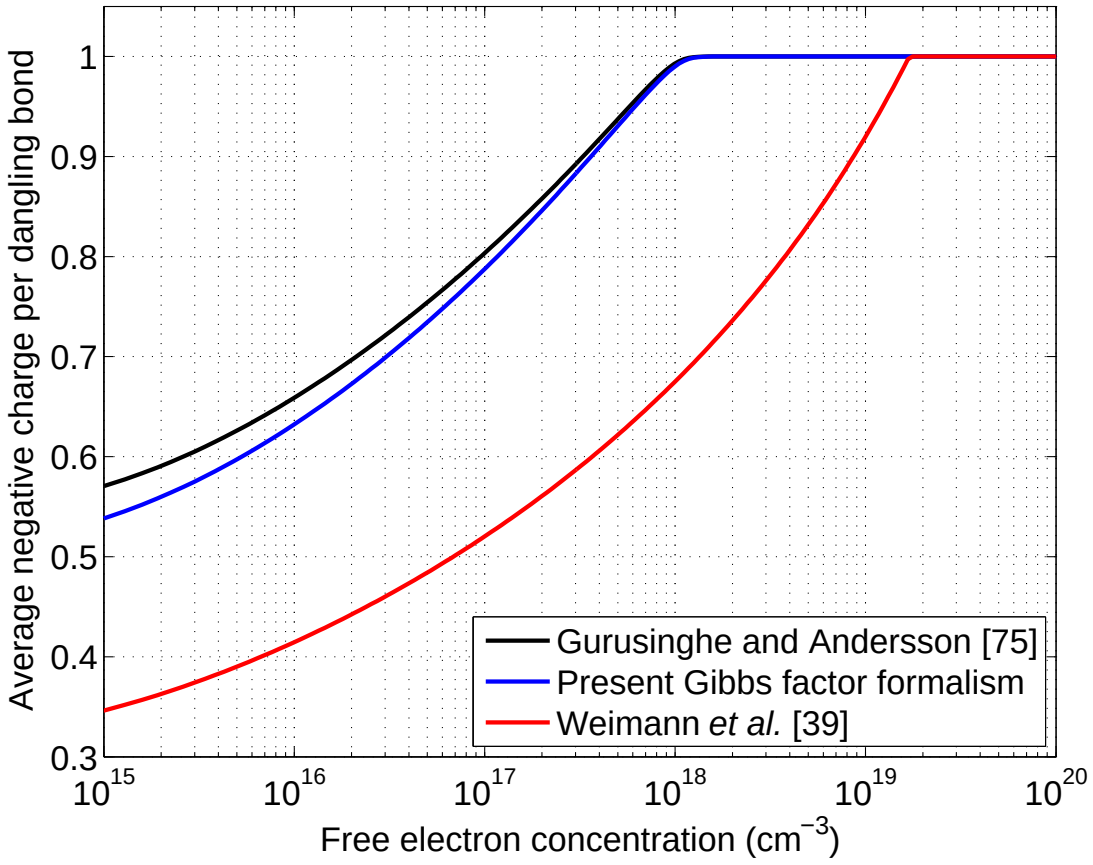

Figure 4.7: The average negative charge per dislocation dangling bond as a function of the free electron concentration within n-type GaN. The calculations were all performed at 300 K for a dislocation line density of 10^8 cm^{-2}.

4.6 Occupation statistics of the $V_{Ga} - O_N$ dislocation core structure within GaN

In this section, another example of the application of the proposed Gibbs factor formalism to the problem of obtaining the occupation statistics of the threading dislocation lines within GaN is provided. In this section, unlike the discussion in Section 4.5, a more realistic $V_{Ga} - O_N$ core structure will be assumed for the threading dislocation lines. The particular atomic configuration of this dislocation core structure was depicted earlier in Figure 1.4(f). It is noted, from Figure 1.4(f), that each of the two small black nitrogen atoms lying beneath the larger white gallium atoms at the center of the $V_{Ga} - O_N$ dislocation defect site, is missing a bonding to a neighbouring atom. This missing bond is due to the gallium vacancy at the defect site, hence the notation, V_{Ga}, in the $V_{Ga} - O_N$ dislocation core structure. These two nitrogen atoms in Figure 1.4(f) are close enough in order to form bonding and anti-bonding states [79]. The energy band configuration of this bonding and anti-bonding energy formation at the $V_{Ga} - O_N$ dislocation defect site is schematically depicted in Figure 4.8.

It is clear from Figure 4.8 that the N-N anti-bonding energy level is the energy level which is electrically active in the $V_{Ga} - O_N$ dislocation core struc-

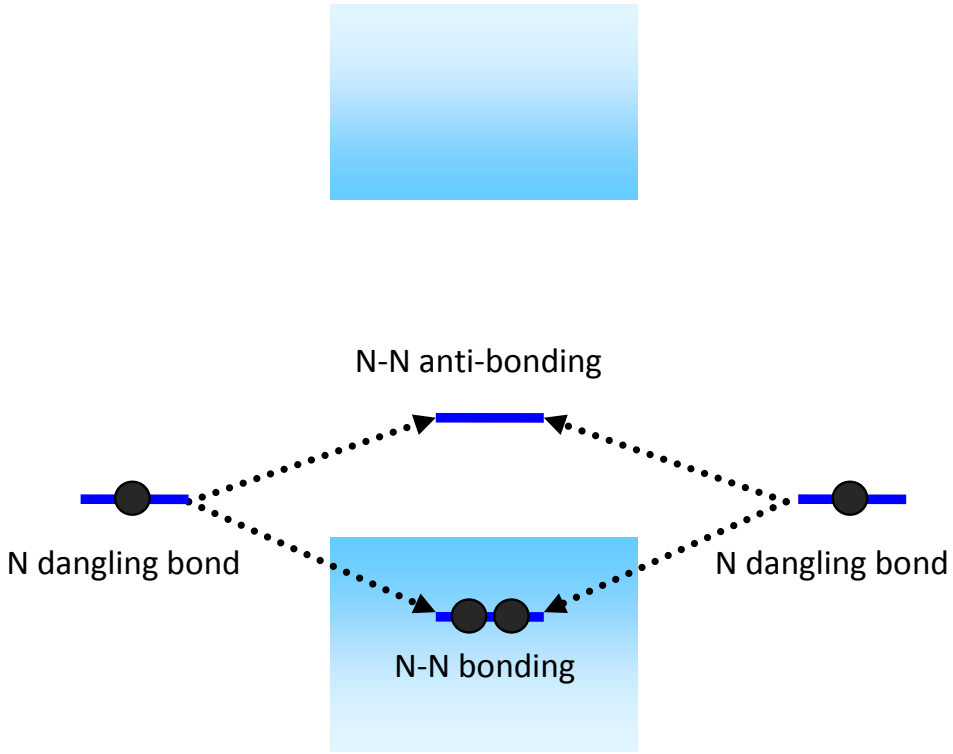

Figure 4.8: Bonding and anti-bonding energy formation from the two nitrogen dangling bonds within the $V_{Ga} - O_N$ dislocation core structure.

ture within GaN. In its neutral state, depicted in Figure 4.8, this energy level holds no electrons, i.e., $i_{s(0)} = 0$. When this energy level is occupied by one electron, it becomes singly negatively charged, i.e., $i_{s(1\downarrow)} = i_{s(1\uparrow)} = -1$, and when it is occupied by two electrons, it becomes doubly negatively charged, i.e., $i_{s(2)} = -2$. For these ionization states, it can be readily shown that the value of the electrostatic potential at the site of a $V_{Ga} - O_N$ dislocation defect will be given by

$$\varphi_o = 2\frac{\varepsilon_0}{q}\Bigg\{-f_{s(1)}\left[\ln\left(N_{s(1)}/2+1\right)+0.577\right]- \\ 2\times f_{s(2)}\left[\ln\left(N_{s(2)}/2+1\right)+0.577\right]+ \\ \frac{2\times f_{s(2)}+f_{s(1)}}{2}\left[1+2\ln\left(\frac{N_{s(2)}c/f_{s(2)}}{R}\right)\right]\Bigg\}. \tag{4.34}$$

Similar to Eq. (4.33), Eq. (4.34) can be solved for the single variable, φ_o, once all the necessary substitutions have been made from the other equations into it. In particular, the inner dislocation defect site electron-electron interactions will be ignored and the value of the dislocation defect energy level, ε_t, will be set to 1.2 eV above the valence band maximum.

After the electrostatic potential, φ_o, has been solved for from Eq. (4.34), its value can be plugged into Eqs. (4.4) through (4.7) in order to obtain the occuption probabilities, $f_{s(0)}$, $f_{s(1)}$, and $f_{s(2)}$ associated with a $V_{Ga} - O_N$ dislocation defect site within GaN. In Figure 4.9, the fraction of the $V_{Ga} - O_N$

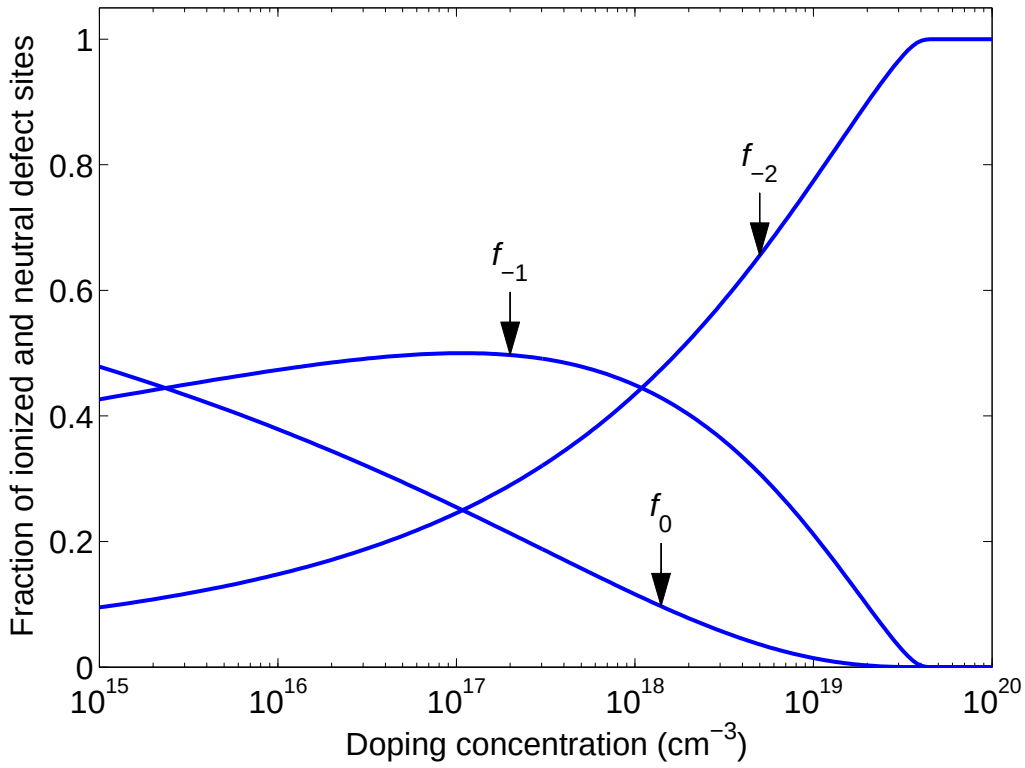

Figure 4.9: The fraction of ionized and neutral dislocation defect sites for the $V_{Ga} - O_N$ core structure of the dislocation lines within n-type GaN as a function of the bulk donor concentration.

dislocation defect sites in their different possible $f_{s(0)}$, $f_{s(1)}$, and $f_{s(2)}$ occupation states have been plotted as a function of the bulk donor concentration; in order to emphasize the charge residing on the dislocation defect sites, in Figure 4.9 the occupation fractions, $f_{s(0)}$, $f_{s(1)}$, and $f_{s(2)}$, have alternatively been labelled as f_0, f_{-1}, and f_{-2}, respectively, these new subscripts representing the corresponding charge states. The material parameters used for these computations are as specified in Table 1.1. These calculations were performed at 300 K for a dislocation line density of 10^8 cm^{-2}. It is found that in the case of the $V_{Ga} - O_N$ dislocation core structure, the Gibbs factor formalism gives a notable computational advantage over the extension of the model of Read [73], as has been pursued by You *et al.* [60, 77]. Furthermore, the application of the Gibbs factor formalism gives a more physically satisfying picture for the occupation of the dislocation lines for this dislocation core structure [79].

In Figure 4.10, the average charge per dislocation defect site, f, is plotted as a function of the free electron concentration, n. For comparison, results corresponding to You *et al.* [60] are also plotted in this figure. It is seen that the overall trends in the two curves depicted in Figure 4.10 are similar. More specifically, at low free electron concentrations, when most of the N-N antibonding energy levels are singly occupied, the differences between the results

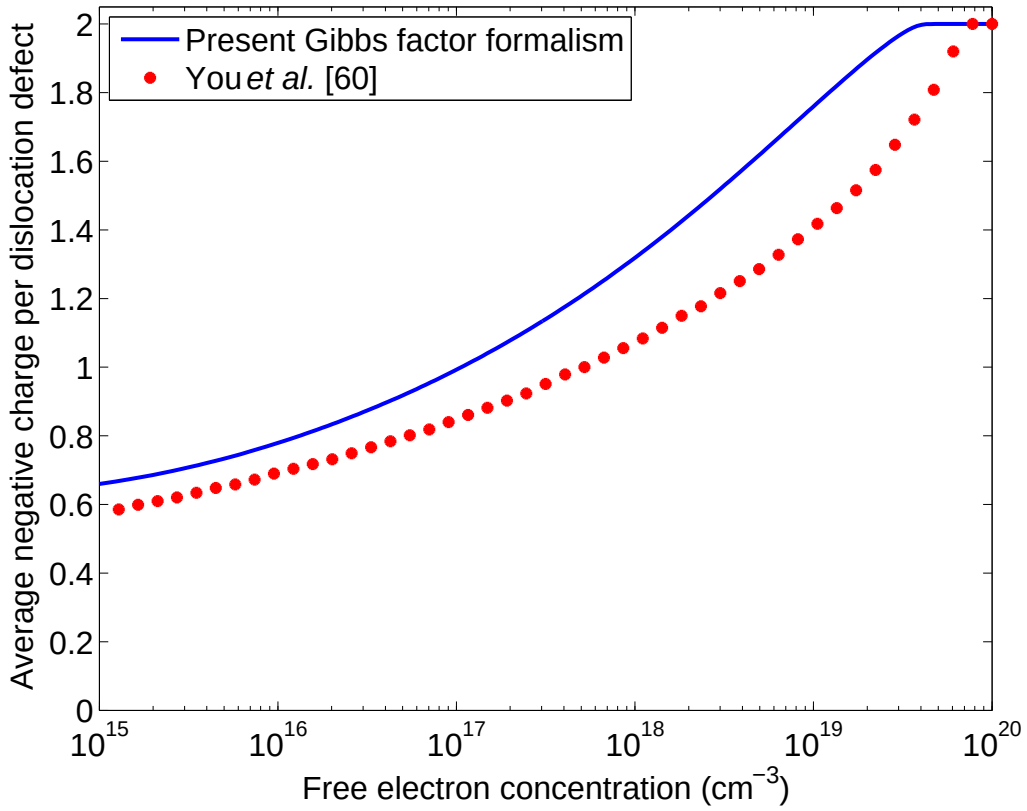

Figure 4.10: The average negative charge per $V_{Ga} - O_N$ dislocation defect site as a function of the free electron concentration within n-type GaN. Results corresponding to the energy minimization approach employed by You *et al.* [60] for the same $V_{Ga} - O_N$ dislocation core structure are also depicted. The results depicted correspond to a temperature of 300 K and a dislocation line density of 10^8 cm^{-2}.

obtained in this thesis and those of You *et al.* [60] are negligible. However, at higher free electron concentrations, when a larger fraction of the N-N anti-bonding energy levels are doubly occupied, differences between the results are more pronounced. As a result, these differences may be attributed to the fact that in the computations of this section, electron-electron interactions within individual N-N anti-bonding energy levels have been neglected when determining the energy associated with the $f_{s(2)}$ occupation state of the N-N anti-bonding energy level.

4.7 Occupation statistics of the open core dislocation core structure within InN

In this section, an open core structure will be assumed for the threading dislocation lines within InN. The atomic configuration of this dislocation core structure was depicted earlier in Figure 1.4(b). The energy band configuration corresponding to this dislocation core structure within InN is depicted in Figure 4.11.

It is clear, from Figure 4.11, that the N-N anti-bonding energy level is the energy level which is electrically active in the open core dislocation core structure within InN. In its neutral state, depicted in Figure 4.11, this energy

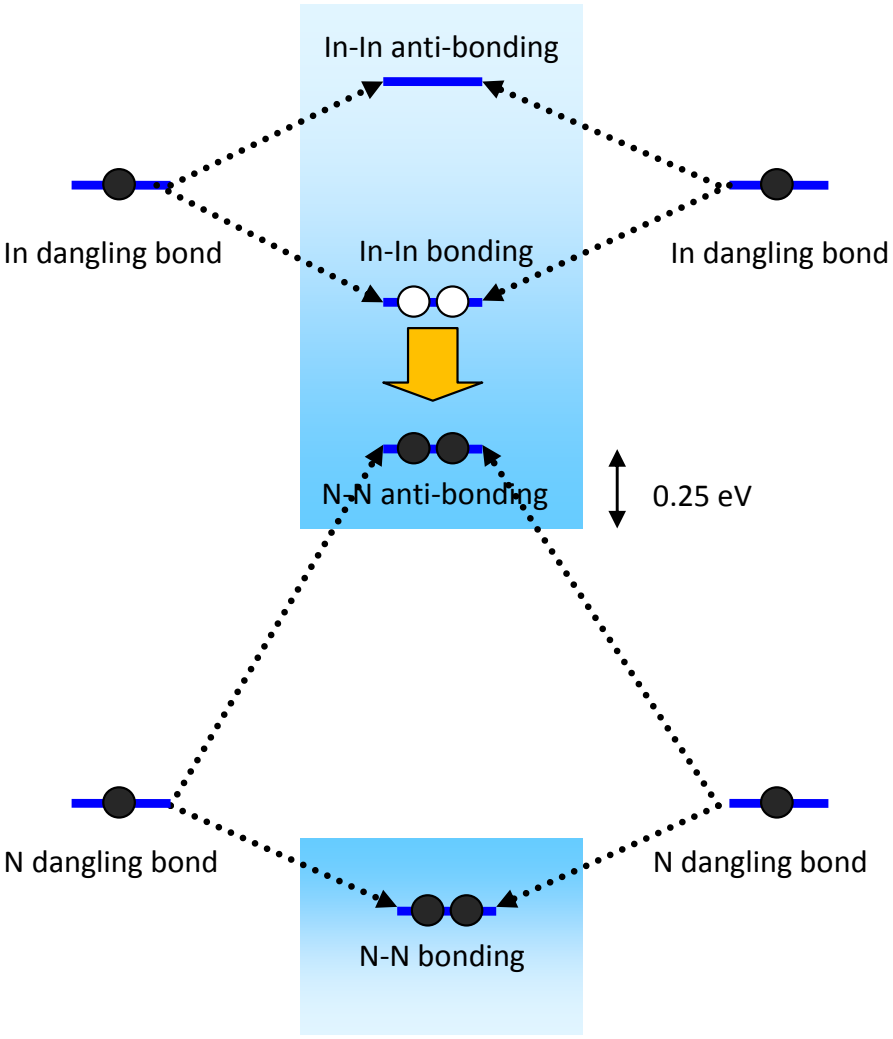

Figure 4.11: Schematic energy band diagram of the neutral state of the open core dislocation core structure within InN.

level holds two electrons, i.e., $i_{s(2)} = 0$. When this energy level loses one of its electrons to the conduction band, it becomes singly positively charged, i.e., $i_{s(1\downarrow)} = i_{s(1\uparrow)} = 1$, and when this energy level holds no electrons it is doubly positively charged, $i_{s(0)} = 2$. For these ionization states, the value of the electrostatic potential at the site of the open core dislocation defect within InN, φ_o, can be obtained as follows

$$\varphi_o = 2\frac{\varepsilon_0}{q}\Bigg\{ f_{s(1)} \left[\ln\left(N_{s(1)}/2+1\right) + 0.577\right] + 2 \times f_{s(2)} \left[\ln\left(N_{s(2)}/2+1\right) + 0.577\right] - \frac{2 \times f_{s(2)} + f_{s(1)}}{2} \left[1 - 0.577 + \ln\left(\frac{\lambda}{N_{s(2)}c/f_{s(2)}}\right)\right]\Bigg\}. \tag{4.35}$$

Note that due to the free electron screening of the positive charge on the dislocation defect sites within InN, Eq. (4.27) has been used to replace $\varphi_{o_{\rm sc}}$ when obtaining the above relation. Similar to Eq. (4.33), Eq. (4.35) can be solved for the single variable, φ_o, once all the necessary substitutions have been made from the other equations into it. For the case of InN, when computing the position of the Fermi energy level, $\varepsilon_{\rm F}$, the slightly different overall charge neutrality condition,

$$N_{\rm d} + f\frac{\sigma_{\rm dis}}{c} = n, \tag{4.36}$$

should be used, due to the fact that within this semiconductor material the dislocation defect sites themselves donate electrons instead of trapping

the electrons donated by the bulk donor atoms; compare Eq. (4.36) with Eq. (4.28). The inner dislocation defect site electron-electron interactions will be ignored. Density functional calculations of Takie and Nakayama [59] have shown that in the open core dislocation core structure within InN, the N-N anti-bonding energy level lies 0.25 eV above the conduction band minimum. As a result, for the purposes of the computations in this section, the dislocation defect energy level, ε_t, will be set equal to 0.25 eV above the conduction band minimum.

After the electrostatic potential, φ_o, has been solved for from Eq. (4.35), its value can be plugged into Eqs. (4.4) through (4.7) in order to obtain the occupation probabilities, $f_{s(0)}$, $f_{s(1)}$, and $f_{s(2)}$, associated with an open core dislocation defect site within wurtzite InN. In Figure 4.12, the fraction of the open core dislocation defect sites in their different possible $f_{s(0)}$, $f_{s(1)}$, and $f_{s(2)}$ occupation states have been plotted as a function of the bulk donor concentration; in order to emphasize the charge residing on the dislocation defect sites, in Figure 4.12 the occupation fractions, $f_{s(0)}$, $f_{s(1)}$, and $f_{s(2)}$, have alternatively been labelled as f_{+2}, f_{+1}, and f_0, respectively, these new subscripts representing the corresponding charge states. The material parameters used for these computations are as specified in Table 1.1. These calculations were performed at 300 K for a dislocation line density of 10^8 cm^{-2}. It is seen

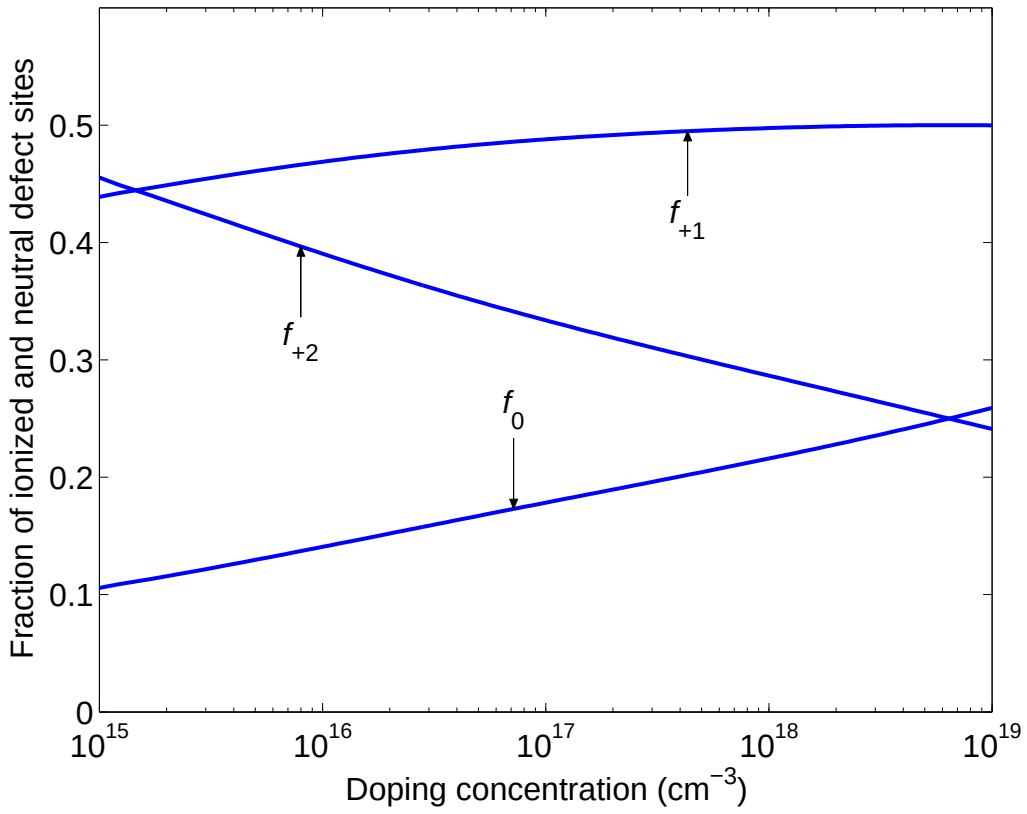

Figure 4.12: The fraction of ionized and neutral dislocation defect sites for the open core structure of the dislocation lines within n-type InN as a function of the bulk donor concentration.

from this figure that, under bulk n-type doping conditions, the dislocation defect sites are predominantly positively charged. In contrast, for the case of n-type GaN, the dislocation defect sites were primarily negatively charged; recall Figures 4.6 and 4.9.

In Figure 4.13, the average positive charge per dislocation defect site for the open core dislocation core structure within wurtzite InN has been plotted as a function of the free electron concentration. In comparison to the dislocation defect occupation statistics results for GaN, obtained in Figures 4.7 and 4.10, it is observed that the average charge per dislocation defect site within InN decreases with increasing free electron concentration. This distinction in the general behavior of the curve depicted in Figure 4.13, when compared to the curves depicted in Figures 4.7 and 4.10, can be attributed to the fact that within n-type GaN, with increasing free electron/bulk donor concentration, the position of the Fermi energy level tends to move away from the position of the dislocation defect energy level. On the other hand, within n-type InN, as the bulk donor concentration/free electron concentration increases, the Fermi energy level moves into the conduction band, and thus, gets closer to the position of the dislocation defect energy level within this semiconductor material.

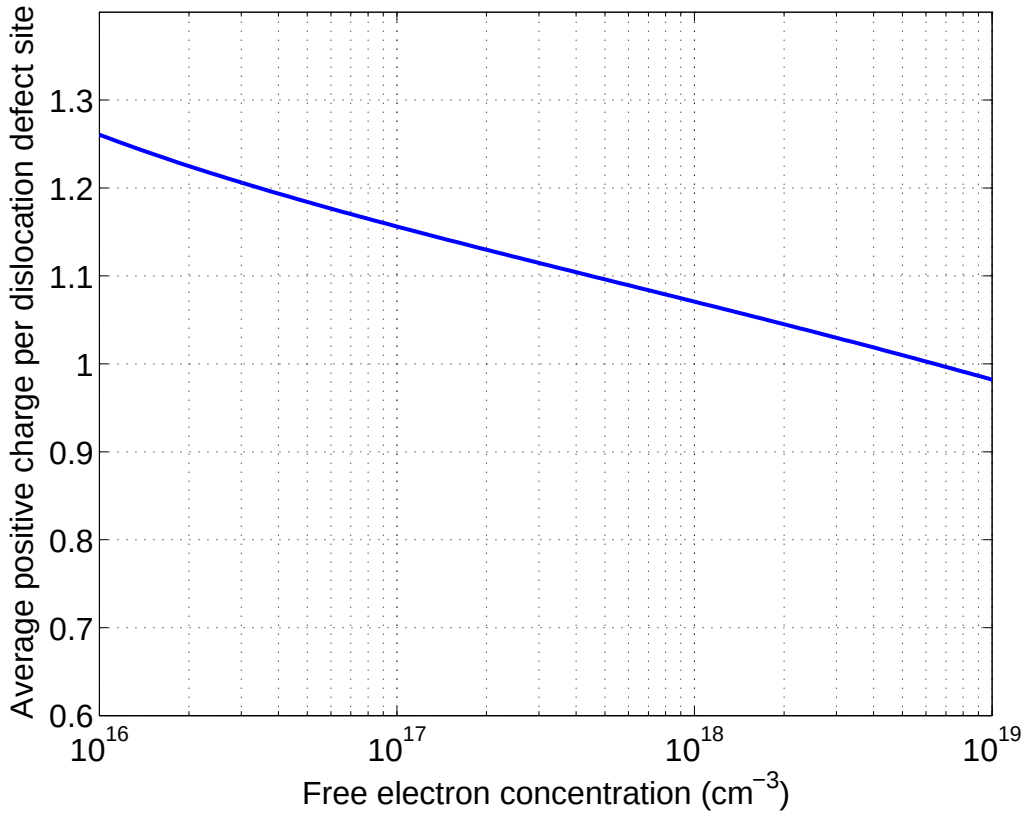

Figure 4.13: The average positive charge per dislocation defect site for the open core structure of the dislocation lines within n-type InN as a function of the free electron concentration. The calculations are performed at 300 K for a dislocation line density of 10^8 cm^{-2}.

Chapter 5

Conclusions

In conclusion, a generalized electrostatic theory of charged dislocation lines within semiconductor materials was developed in this thesis. Specifically, the generalizations involved, allow for a determination of the occupation statistics of multiple ionization states of the defect sites along a dislocation line. In addition, the formulation developed in this thesis allows for the determination of the most general screening space charge profile associated with the dislocation lines [80]. The materials considered in this analysis were the nitride based semiconductors, GaN and InN, for which strained epitaxial crystal growth results in the presence of a high density of threading dislocation lines within their respective crystal structures.

It was found that the distinctively different positionings of the disloca-

tion defect energy levels relative to the conduction band minimum in the two semiconductor materials, GaN and InN, lead to distinctively different profiles for the space charge distribution, screening the threading dislocation line charge in each material; while within n-type GaN, the screening is dominated by ionized bulk donor atoms, within n-type InN, this screening is provided for by the free electrons donated by the defect sites situated along the threading dislocation line itself. The recognition of this distinction in the screening space charge distribution of the threading dislocation lines within InN when compared to the case of GaN was missing in the literature and its computation has thus been one of the original contributions of this research.

The dislocation limited electron drift and Hall mobilities within GaN and InN were also computed as part of this research. Under the same n-type bulk doping conditions, it was observed that the electron drift and Hall mobilities within InN are much higher than those computed for the case of GaN. This higher electron mobility within InN can be attributed to the much stronger screening of the dislocation core charge within InN as well as the lower value for the electron effective mass of InN. Current experimental data existing in the literature on the threading dislocation line density dependence of the electron Hall mobility within InN, differ by an order of magnitude [66, 67] and furthermore, within each experimental data set, are much too scattered

to enable a conclusive comparison with the theoretically computed values in this thesis for the electron Hall mobility within InN. Nevertheless, in the future, as the quality of the epitaxially grown layers of InN improve, and more accurate experimental determinations of the electron Hall mobility within InN are performed, it is expected that the theoretical results obtained in this thesis will provide a conclusive answer as to how much charge is accumulated along the threading dislocation lines. This is important, because of the fact that the threading dislocation lines within InN have been blamed for the high unintentional n-type conductivity of InN. This high unintentional n-type conductivity is in turn hampering the successful p-type doping of this important semiconductor material and thus, the fabrication of functional electronic/optoelectronic devices from InN.

The application of the Gibbs factor formalism to the problem of determining the occupation statistics of the defect sites along a dislocation line has been another original contribution of this work. It was shown that in special cases the formulation essentially reduces to the model of Read [73] for the treatment of the dislocation lines.

In continuation of the work presented in this thesis, several avenues for future investigation are conceivable. These topics for further investigation include the following:

(1) In the literature, only limiting case analytical expressions have been used in order to obtain the electron drift mobility limited by scattering from the threading dislocation lines within GaN [39, 40, 75]. The scattering potential that has been computed in this thesis, as well as experimental data from the literature [69, 71], suggest that the actual scattering potential deviates substantially from the simple limiting case analytical expressions used in the literature for the purposes of computing the dislocation limited electron mobility within GaN.

(2) In Section 3.2, when formulating the dislocation limited electron drift and Hall mobilities, it was assumed that the dislocation lines are well separated from each other. Under high threading dislocation line density conditions, i.e., when the screening space charge cylinders of nearby dislocation lines start to overlap, this assumption of the formulation developed in Chapter 3 will no longer be valid. Furthermore, under high dislocation line density conditions, the occupation statistics of the threading dislocation lines obtained in Chapter 4 relies on the implicit assumption that the dislocation lines are uniformly distributed within the semiconductor sample. Thus, in the high dislocation line density limit, a more rigorous treatment of the effect of non-uniformity in the distribution of the threading dislocation lines, on both the free carrier concentration and the electron mobility, remains to be

addressed.

References

[1] S. Nakamura, "InGaN/AlGaN blue-light-emitting diodes," *J. Vac. Sci. Technol. A*, vol. 13, no. 3, pp. 705-710, May/June 1995.

[2] S. Nakamura, "The roles of structural imperfections in InGaN-based blue light-emitting diodes and laser diodes," *Science*, vol. 281, pp. 956-961, August 1998.

[3] S. Strite and H. Morkoç, "GaN, AlN, and InN: A review," *J. Vac. Sci. Technol. B*, vol. 10, no. 4, pp. 1237-1266, July/August 1992.

[4] H. Morkoç, S. Strite, G. B. Gao, M. E. Lin, B. Sverdlov, and M. Burns, "Large-band-gap SiC, III-V nitride, and II-VI ZnSe-based semiconductor device technologies," *J. Appl. Phys.*, vol. 76, no. 3, pp. 1363-1398, August 1994.

[5] S. N. Mohammad and H. Morkoç, "Progress and prospects of group-III nitride semiconductors," *Prog. Quantum Electron.*, vol. 20, no. 5/6, pp. 361-525, 1996.

[6] S. J. Pearton, J. C. Zolper, R. J. Shul, and F. Ren, "GaN: Processing, defects, and devices," *J. Appl. Phys.*, vol. 86, no. 1, pp. 1-78, July 1999.

[7] J. Q. Wu, "When group-III nitrides go infrared: New properties and perspectives," *J. Appl. Phys.*, vol. 106, pp. 011101-1-28, July 2009.

[8] F. A. Ponce, and D. P. Bour, "Nitride-based semiconductors for blue and green light-emitting devices," *Nature*, vol. 386, pp. 351-359, March 1997.

[9] U. K. Mishra, L. Shen, T. E. Kazior, and Y.-F. Wu, "GaN-based rf power devices and amplifiers," *Proceedings of the IEEE*, vol. 96, no. 2, pp. 287-305, February 2008.

[10] W. C. Johnson, J. B. Parsons, and M. C. Crew, "Nitrogen compounds of gallium. III," *J. Phys. Chem.*, vol. 36, no. 10, pp. 2651-2654, January 1932.

[11] H. J. Hovel and J. J. Cuomo, "Electrical and optical properties of rf-sputtered GaN and InN," *Appl. Phys. Lett.*, vol. 20, no. 2, pp. 71-73, January 1972.

[12] K. V. Malyutin and A. A. Veshkin, "Preparation of GaN films by cathodic sputtering," *Neorg. Mater.*, vol. 8, no. 5, pp. 821-823, May 1972.

[13] J. C. Vesely, M. Shatzkes, and P. J. Burkhard, "Space-charge-limited current flow in gallium nitride thin films," *Phys. Rev. B*, vol. 10, no. 2, pp. 582-590, July 1974.

[14] T. Hariu, T. Usuba, H. Adachi, and Y. Shibata, "Reactive sputtering of gallium nitride thin films for GaAs MIS structures," *Appl. Phys. Lett.*, vol. 32, no. 4, pp. 252-253, February 1978.

[15] E. Lakshmi, B. Mathur, A. B. Bhattacharya, and V. P. Bhargava, "The growth of highly resistive gallium nitride films," *Thin Solid Films*, vol. 74, no. 1, pp. 77-82, December 1980.

[16] K. Matsushita, Y. Matsuno, T. Hariu, and Y. Shibata, "A comparative study of the deposition conditions in the plasma-assisted deposition of gallium nitride thin films," *Thin Solid Films*, vol. 80, no. 1-3, pp. 243-247, June 1981.

[17] K. Kubota, Y. Kobayashi, and K. Fujimoto, "Preparation and properties of III-V nitride thin films," *J. Appl. Phys.*, vol. 66, no. 7, pp. 2984-2988, October 1989.

[18] H. P. Maruska and J. J. Tietjen, "The preparation and properties of vapor-deposited single-crystal-line GaN," *Appl. Phys. Lett.*, vol. 15, no. 10, pp. 327-329, November 1969.

[19] J. I. Pankove, J. E. Berkeyheiser, H. P. Maruska, and J. Wittke, "Luminescent properties of GaN," *Solid State Commun.*, vol. 8, no. 13, pp. 1051-1053, July 1970.

[20] R. K. Crouch, W. J. Debnam, and A. L. Fripp, "Properties of GaN grown on sapphire substrates," *J. Mater. Sci.*, vol. 13, no. 11, pp. 2358-2364, 1978.

[21] A. S. Adonin, V. A. Evmenenko, L. N. Mikhailov, and N. G. Ryabtsev, "Study of certain kinetic features of the growth and doping of heteroepitaxial layers of gallium nitride, their cathodoluminescence and electric properties," *Neorg. Mater.*, vol. 17, no. 9, pp. 1608-1613, September 1981.

[22] R. Juza and H. Hahn, "Crystal structures of Cu_3N, GaN and InN - Metallic amides and metallic nitrides V Announcement," *Zeitschr. Anorgan. Allgem. Chem.*, vol. 239, no. 3, pp. 282-287, October 1938.

[23] J. Pastrnak and L. Souckova, "Production of thin layers of aluminum, gallium and indium nitride under a gas discharge," *Phys. Status Solidi*, vol. 3, no. 2, pp. K71-K74, 1963.

[24] T. L. Tansley and C. P. Foley, "Electron mobility in indium nitride," *Electron. Lett.*, vol. 20, no. 25-26, pp. 1066-1068, December 1984.

[25] L. A. Marasina, I. G. Pichugin, and M. Tlaczala, "Preparation of InN epitaxial layers in $InCl_3 - NH_3$ system," *Krist. Technol.*, vol. 12, no. 6, pp. 541-455, January 1977.

[26] H. Lu, W. J. Schaff, and L. F. Eastman, "Surface charge accumulation of InN films grown by molecular-beam epitaxy," *Appl. Phys. Lett.*, vol. 82, no. 11, pp. 1736-1768, March 2003.

[27] V. Y. Davydov, A. A. Klochikhin, R. P. Seisyan, V. V. Emtsev, S. V. Ivanov, F. Bechstedt, J. Furthmuller, H. Harima, A. V. Mudryi, J. Aderhold, O. Semchinova, and J. Graul, "Absorption and emission of hexagonal InN. Evidence of narrow fundamental band gap," *Phys. Status Solidi (b)*, vol. 229, no. 3, pp. r1-r3, February 2002.

[28] T. L. Tansley and C. P. Foley, "Optical band gap of indium nitride," *J. Appl. Phys.*, vol. 59, no. 9, pp. 3241-3244, May 1986.

[29] V. A. Tyagai, A. M. Evstigneev, A. N. Krasiko, A. F. Andreeva, and V. Y. Malakhov, "Optical properties of indium nitride films," *Sov. Phys. Semicond.*, vol. 11, no. 11, pp. 1257-1259, November 1977.

[30] K. L. Westra, R. P. W. Lawson, and M. J. Brett, "The effects of oxygen contamination on the properties of reactively sputtered indium nitride films," *J. Vac. Sci. Technol. A*, vol. 6, no. 3, pp. 1730-1732, May/June 1988.

[31] Y. E. Romanyuk, D. Kreier, Y. Cui, K. M. Yu, J. W. Ager III, and S. R. Leone, "Molecular beam epitaxy of InGaN thin films on Si(111): Effect of substrate nitridation," *Thin Solid Films*, vol. 517, no. 24, pp. 6512-6515, October 2009.

[32] K. P. Beh, F. K. Yam, C. W. Chin, S. S. Tneh, and Z. Hassan, "The growth of III-V nitrides heterostructure on Si substrate by plasma-assisted molecular beam epitaxy," *J. Alloys Compd.*, vol. 506, no. 1, pp. 343-346, September 2010.

[33] M. Kurouchi, T. Yamaguchi, H. Naoi, A. Suzuki, T. Araki, and Y. Nanishi, "Growth of In-rich InGaN on InN template by radio-frequency

plasma assisted molecular beam epitaxy," *J. Cryst. Growth*, vol. 275, no. 1-2, pp. e1053-e1058, February 2005.

[34] N. Li, S. -J. Wang, E. -H. Park, Z. C. Feng, H. -L. Tsai, J. -R. Yang, and I. Ferguson, "Suppression of phase separation in InGaN layers grown on lattice-matched ZnO substrates," *J. Cryst. Growth*, vol. 311, no. 22, pp. 4628-4631, November 2009.

[35] D. Kapolnek, X. H. Wu, B. Heying, S. Keller, B. P. Keller, U. K. Mishra, S. P. Den Baars, and J. S. Speck, "Structural evolution in epitaxial metalorganic chemical vapor deposition grown GaN films on sapphire," *Appl. Phys. Lett.*, vol. 67, no. 11, pp. 1541-1543, September 1995.

[36] F. A. Ponce, B. S. Krusor, J. S. Major, Jr., W. E. Plano, and D. F. Welch, "Microstructure of GaN epitaxy on SiC using AlN buffer layers," *J. Appl. Phys.*, vol. 67, no. 3, pp. 410-412, July 1995.

[37] V. Cimalla, V. Lebedev, F. M. Morales, M. Niebelschütz, G. Ecke, R. Goldhahn, and O. Ambacher, "Origin of n-type conductivity in nominally undoped InN," *Mat.-wiss. u. Werkstofftech*, vol. 37, No. 11, pp. 924-928, November 2006.

[38] R. Jaszek, "Carrier scattering by dislocations in semiconductors," *J. Mater. Sci.: Mater. Electron.*, vol. 12, no. 1, pp. 1-9, 2001.

[39] N. G. Weimann, L. F. Eastman, D. Doppalapudi, H. M. Ng, and T. D. Moustakas, "Scattering of electrons at threading dislocations in GaN," *J. Appl. Phys.*, vol. 83, no. 7, pp. 3656-3659, April 1998.

[40] D. C. Look, and J. R. Sizelove, "Dislocation scattering in GaN," *Phys. Rev. Lett.*, vol. 82, no. 6, pp. 1237-1240, February 1999.

[41] F. A. Ponce, D. P. Bour, W. Gotz, and P. J. Wright, "Spatial distribution of the luminescence in GaN thin films," *Appl. Phys. Lett.*, vol. 68, no. 1, pp. 57-59, January 1996.

[42] T. Lei, M. Fanciulli, R. J. Molnar, T. D. Moustakas, R. J. Graham, and J. Scanlon, "Epitaxial growth of zinc blende and wurtzitic gallium nitride thin films on (001) silicon," *Appl. Phys. Lett.*, vol. 59, no. 8, pp. 944-946, August 1991.

[43] S.-H. Park and S.-L. Chuang, "Comparison of zinc-blende and wurtzite GaN semiconductors with spontaneous polarization and piezoelectric field effects," *J. Appl. Phys.*, vol. 87, no. 1, pp. 353-364, January 2000.

[44] M. E. Levinshtein, S. L. Rumyantsev, and M. Shur, *Properties of Advanced Semiconductor Materials: GaN, AlN, InN, BN, SiC, SiGe.* New York: John Wiley and Sons Inc., pp. 1-30, 2001.

[45] T. Unishima, M. Highashiwaki, and T. Matsui, "Optical properties of Si-doped InN grown on sapphire (0001)," *Phys. Rev. B*, vol. 68, no. 23, pp. 235204-1-7, December 2003.

[46] J. Wu, W. Walukiewicz, K. M. Yu, J. W. Ager, E. E. Haller, H. Lu, W. J. Schaff, Y. Saito, and Y. Nanishi, "Unusual properties of the fundamental band gap of InN," *Appl. Phys. Lett.*, vol. 80, no. 21, pp. 3967-3969, May 2002.

[47] H. Wang, and A.-B. Chen, "Calculation of shallow donor levels in GaN," *J. Appl. Phys.*, vol. 87, no. 11, pp. 7859-7863, June 2000.

[48] A. Janotti and C. G. Van de Walle, "Sources of unintentional conductivity in InN," *Appl. Phys. Lett.*, vol. 92, pp. 032104-1-3, January 2008.

[49] M. E. Levinshtein, S. L. Rumyantsev, and M. Shur, *Properties of Advanced Semiconductor Materials: GaN, AlN, InN, BN, SiC, SiGe*. New York: John Wiley Sons Inc., pp. 49-66, 2001.

[50] O. Lagerstedt and A. Monemar, "Variation of lattice parameters in GaN with stoichiometry and doping," *Phys. Rev. B*, vol. 19, no. 6, pp. 3064-3070, March 1979.

[51] I. G. Pichugin and M. Tlachala, "X-Ray analysis of indium nitride," *Inorg. Mater.*, vol. 14, no. 1, pp. 135-136, 1978.

[52] David Darling, "The encyclopaedia of science, Solid State Physics" *http://www.daviddarling.info/encyclopedia/D/dislocation.html*

[53] X. H. Wu, L. M. Brown, K. Kapolnek, S. Keller, B. Keller, S. P. DenBaars, and J. S. Speck, "Defect structure of metal-organic chemical vapor deposition-grown epitaxial (0001) GaN/Al_2O_3," *J. Appl. Phys.*, vol. 80, no. 6, pp. 3228-3237, September 1996.

[54] T. Hino, S. Tomiya, T. Miyajima, K. Yanashima, S. Hashimoto, and M. Ikeda, "Characterization of threading dislocations in GaN epitaxial layers," *Appl. Phys. Lett.*, vol. 76, no. 23, pp. 3421-3423, June 2000.

[55] J. Arvanitidis, D. Christofilos, G. A. Kourouklis, A. Delimitis, M. Katsikini, P. Komninou, S. Ves, E. Dimakis, and A. Georgakilas, "Depth profile of the biaxial strain in a 10 μm thick InN (0001) film," *J. Appl. Phys.*, vol. 100, pp. 113516-1-5, December 2006.

[56] C. Rauch, F. Tuomisto, A. V. Clemente, B. Lacroix, P. Ruterana, S. Kraeusel, B. Hourahine, and W. J. Schaff, "Defect evolution and interplay in n-type InN," *Appl. Phys. Lett.*, vol. 100, pp. 091907-1-3, March 2012.

[57] S. M. Lee, M. A. Belkhir, X. Y. Zhu, Y. H. Lee, Y. G. Hwang and T. Frauenheim, "Electronic structures of GaN edge dislocations," *Phys. Rev. B*, vol. 61, no. 23, pp. 16033-16039, June 2000.

[58] L. Lymperakis, J. Neugebauer, M. Albrecht, T. Remmele, and H. P. Strunk, "Strain induced deep electronic states around threading dislocations in GaN," *Phys. Rev. Lett.*, vol. 93, no. 19, pp. 196401-1-4, November 2004.

[59] Y. Takei and T. Nakayama, "Electron-carrier generation by edge dislocations in InN films: First-principles study," *J. Cryst. Growth*, vol. 311, no. 10, pp. 2767-2771, May 2009.

[60] J. H. You, J. Q. Lu, and H. T. Johnson, "Electron scattering due to threading edge dislocations in n-type wurtzite GaN," *J. Appl. Phys.*, vol. 99, pp. 033706-1-10, February 2006.

[61] E. Kalesaki, J. Kioseoglou, L. Lymperakis, P. Komninou, and T. Karakostas, "Effect of edge threading dislocations on the electronic structure of InN," *Appl. Phys. Lett.*, vol. 98, pp. 072103-1-3, February 2011.

[62] C. J. Gallagher, "Plastic deformation of germanium and silicon," *Phys. Rev.*, vol. 88, no. 4, pp. 721-722, November 1952.

[63] G. L. Pearson, W. T. Read, and F. J. Morin, "Dislocations in plastically deformed germanium," *Phys. Rev.*, vol. 93, no. 4, pp. 666-667, February 1954.

[64] W. Schröter and H. Cerva, "Interaction of point defects with dislocations in silicon and germanium: Electrical and optical effects," *Solid State Phenom.*, vol. 85-86, pp. 67-143, 2002.

[65] C. Shi, P. M. Asbeck, and E. T. Yu, "Piezoelectric polarization associated with dislocations in wurtzite GaN," *Appl. Phys. Lett.*, vol 74, no. 4, pp. 573-575, January 1999.

[66] H. Wang, D. S. Jiang, L. L. Wang, X. Sun, W. B. Liu, D. G. Zhao, J. J. Zhu, Z. S. Liu, Y. T. Wang, S. M. Zhang, and H. Yang, "Investigation on the structural origin of n-type conductivity in InN films," *J. Phys. D: Appl. Phys.*, vol. 41, no. 13, pp. 135403-1-5, June 2008.

[67] C. S. Gallinat, G. koblmüller, and J. S. Speck, "The role of threading dislocations and unintentionally incorporated impurities on the bulk electron conductivity of In-face InN," *Appl. Phys. Lett.*, vol. 95, pp. 022103-1-3, July 2009.

[68] J. Cai and A. Ponce, "Determination by electron holography of the electronic charge distribution at threading dislocations in epitaxial GaN," *Phys. Stat. Sol. (a)*, vol. 192, no. 2, pp. 407-411, July 2002.

[69] D. Cherns, C. G. Jiao, H. Mokhtari, J. Cai, and F. A. Ponce, "Electron holography studies of the charge on dislocations in GaN," *Phys. Stat. Sol. (b)*, vol. 234, no. 3, pp. 924-930, December 2002.

[70] B. S. Simpkins, E. T. Yu, P. Waltereit, and J. S. Speck, "Correlated scanning Kelvin probe and conductive atomic force microscopy studies of dislocations in gallium nitride," *J. Appl. Phys.*, vol. 94, no. 3, pp. 1448-1453, August 2003.

[71] E. Müller, D. Gerthsen, P. Brückner, F. Scholz, T. Gruber, and A. Waag, "Probing the electrostatic potential of charged dislocations in n-GaN and n-ZnO epilayers by transmission electron holography," *Phys. Rev. B*, vol. 73, no. 24, pp. 245316-1-9, June 2006.

[72] L. F. J. Piper, T. D. Veal, C. F. McConville, H. Lu, and W. J. Schaff, "Origin of the n-type conductivity of InN: The role of positively charged dislocations," *Appl. Phys. Lett.*, vol. 88, pp. 252109-1-3, June 2006.

[73] W. T. Read, Jr., "Theory of dislocations in germanium," *Philos. Mag.*, vol. 45, no. 367, pp. 775-796, August 1954.

[74] J. Singh, *Electronic and Optoelectronic Properties of Semiconductor Structures.*, Cambridge: Cambridge University Press, Chapter 4, 2003.

[75] M. N. Gurusinghe and T. G. Andersson, "Mobility in epitaxial GaN: Limitations of free-electron concentration due to dislocations and compensation," *Phys. Rev. B*, vol. 67, no. 23, pp. 235208-1-7, June 2003.

[76] K. Leung, A. F. Wright, and E. B. Stechel, "Charge accumulation at a threading edge dislocation in gallium nitride," *Appl. Phys. Lett.*, vol. 74, no. 17, pp. 2495-2497, April 1999.

[77] J. H. You, J. Q. Lu, and H. T. Johnson, "Atomistically informed electrostatic model of an edge dislocation in a complex crystalline material," *Mathematics and Mechanics of Solids*, vol. 13, no. 3-4, pp. 267-291, May 2008.

[78] E. Baghani and S. K. O'Leary, "Occupation statistics of dislocations within uncompensated n-type wurtzite gallium nitride," *J. Appl. Phys.*, vol. 109, pp. 113706-1-6, June 2011.

[79] E. Baghani and S. K. O'Leary, "Occupation statistics of the $V_{Ga} - O_N$ dislocations within n-type gallium nitride," *J. Appl. Phys.*, vol. 110, pp. 033509-1-6, August 2011.

[80] E. Baghani and S. K. O'Leary, "Electron mobility limited by scattering from screened positively charged dislocation lines within indium nitride," *Appl. Phys. Lett.*, vol. 99, pp. 262106-1-3, December 2011.

Appendices

Appendix A. Iterative procedure for solving the screening space charge distribution within GaN

The iterative procedure described in this and the following appendix, is based upon finding successively more accurate solutions to the screening space charge distribution function, $n_{\rm sc}(r)$. For concreteness, in the example solved in this appendix, the value of f has been fixed to 1, i.e., it is assumed that on average, one electron is being trapped per dislocation defect site. The bulk donor concentration, $N_{\rm d}$, has been fixed to the representative value of 10^{18} cm $^{-3}$. The same procedure described in this appendix can be readily applied in order to obtain an accurate approximation to the screening space charge distribution function, $n_{\rm sc}(r)$, for other values of f and $N_{\rm d}$ as

well. Throughout this appendix, the dislocation core charge cylinder will be assumed to be the same as that defined earlier, i.e., in Eq. (2.1).

In the case of the screening of the dislocation core charge within GaN, the model of Read [73] provides us with a first approximation to the screening space charge distribution function, $n_{\rm sc}(r)$, i.e.,

$$n_{\rm sc}(r) \approx \begin{cases} N_{\rm d}, & r \leq R \\ 0, & r > R \end{cases} , \tag{A.1}$$

where the Read radius, R, is defined in Section 4.3. This approximate screening space charge distribution function is depicted with the blue curve in Figure A.1(a). Substitution of the approximate screening space charge distribution function from Eq. (A.1) into Eq. (2.9) and subsequently, the resultant electrostatic potential into Eqs. (2.10) and (2.11), yields a new screening space charge distribution function depicted by the red curve in Figure A.1(a). If the screening space charge distribution suggested in Eq. (A.1) were the exact simultaneous solution of Eqs. (2.3) and (2.9), the blue and red curves in Figure A.1(a) would coincide.

From Figure A.1(a) it is noted that when compared with the blue curve, the red curve in this figure is deficient in the amount of positive charge contained within it. As a result, the space charge distribution function depicted with the red curve in Figure A.1(a) does not meet the charge neutrality condition, i.e., the total amount of positive charge contained within it does not

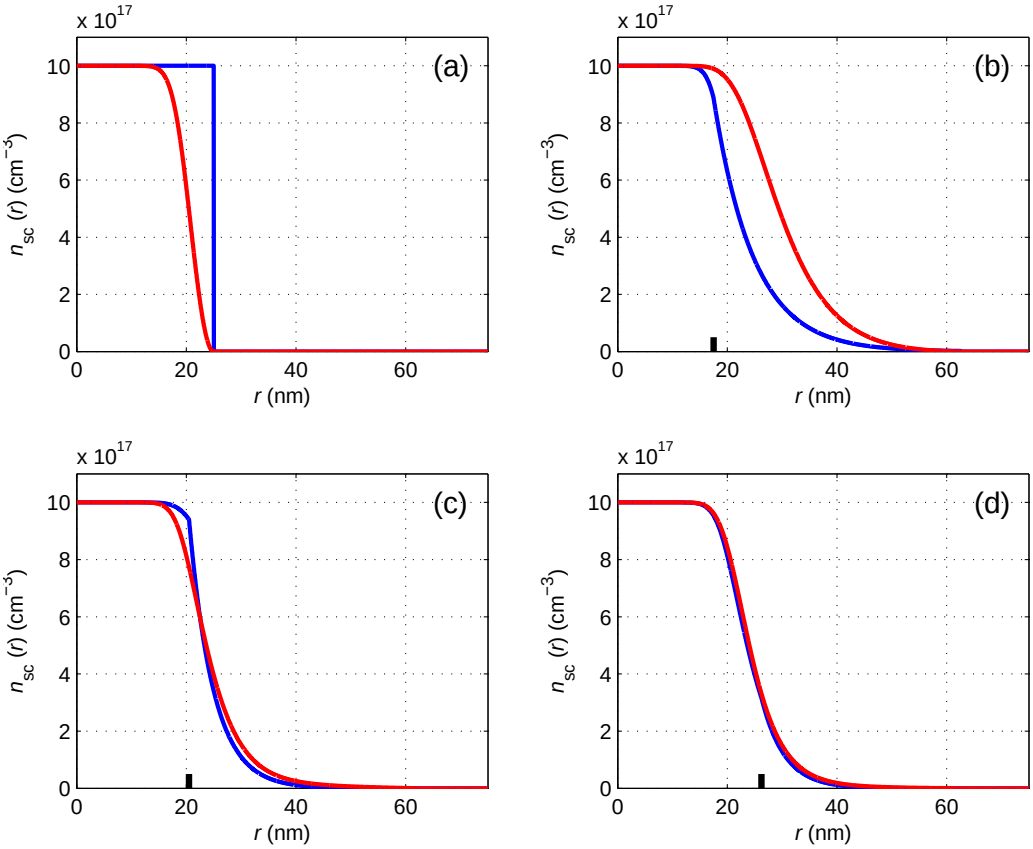

Figure A.1: An iterative construction of the screening space charge surrounding a threading dislocation line within n-type GaN.

exactly equal the fixed negative charge within the dislocation core charge cylinder.

For the next suggested approximation to the screening space charge distribution function, $n_{\mathrm{sc}}(r)$, this deficiency in the net positive charge needs to be remedied. In order to compensate for this deficiency, in the next suggested approximation for the screening space charge distribution, part of the red curve from Figure A.1(a) is replaced by an exponential tail at radial distances above a truncation radius, r_{trunc}, indicated by the black line on the horizontal axis in Figure A.1(b). In other words, for $0 \leq r < r_{\mathrm{trunc}}$, the new suggested approximation to the screening space charge distribution function, $n_{\mathrm{sc}}(r)$, is identical to the red curve in Figure A.1(a). For $r_{\mathrm{trunc}} \leq r < R_{\mathrm{sc}}$, this new suggested approximation is simply an exponential function, $A\exp(-r/\lambda)$. The two variables, A and λ, can be uniquely determined by the requirement that: (1) $n_{\mathrm{sc}}(r)$ should remain continuous at r_{trunc}, and (2) the total negative charge subtended by the newly suggested approximation to $n_{\mathrm{sc}}(r)$ should be equal to the fixed negative charge in the dislocation core charge cylinder. The resultant screening space charge distribution is depicted by the blue curve in Figure A.1(b). Subsequent substitution of the screening space charge distribution depicted by the blue curve in Figure A.1(b) into Eqs. (2.9), (2.10), and (2.11), yields the red curve depicted in Figure A.1(b).

In Figures A.1(c) and A.1(d), the same process of replacing an exponential tail to the red curve from the previous iteration has been repeated. The radius at which the exponential tail is replaced in each iteration has been chosen so that improved convergence between the blue and red curves in successive iterations is maintained. It is observed that sufficient convergence is reached in Figure A.1(d), i.e., a self-consistent solution to Eqs. (2.3) and (2.9) has been found.

Appendix B. Iterative procedure for solving the screening space charge distribution within InN

For concreteness, in the example solved in this appendix, the value of f has been fixed to 1, i.e., it is assumed that on average, each dislocation defect site donates one electron. The bulk donor concentration, $N_{\rm d}$, has been fixed to the representative value of 10^{18} cm $^{-3}$. The same procedure described in this appendix can be readily applied in order to obtain an accurate approximation to the screening space charge distribution function, $n_{\rm sc}(r)$, for other values of f and $N_{\rm d}$ as well. Throughout this appendix, the dislocation core charge cylinder will be assumed to be the same as that defined earlier, i.e., in Eq. (2.1).

In the case of InN, the screening of the dislocation core charge is provided for by the free electrons donated by the dislocation defect sites. As their name suggests, free electrons are free to aggregate around the positive charge on the dislocation core charge cylinder. Consequently, the free electron concentration is expected to be higher near the dislocation core and to drop off at radial distances further away from the dislocation line. The process may thus be initiated by approximating such screening space charge

distribution by a simple exponential function, i.e.,

$$n_{\mathrm{sc}}(r) \approx n_0 \exp(-r/\lambda). \tag{B.1}$$

Initially, the value of λ is set equal to the degenerate Debye length within the bulk of InN, which for the free electron concentration of 10^{18} cm^{-3}, equals 10.57 nm. The other unknown variable in Eq. (B.1), namely, n_0, is uniquely determined from the requirement that the total negative charge subtended by the screening space charge distribution, $n_{\mathrm{sc}}(r)$, equals the positive charge within the dislocation core charge cylinder. This suggested screening space charge distribution is depicted with the blue curve in Figure B.1(a).

Substituting the screening space charge distribution function, $n_{\mathrm{sc}}(r)$, from Eq. (B.1) into Eq. (2.9), the electrostatic potential resulting from this space charge distribution, screening the dislocation core charge, can be obtained. Substituting the resultant electrostatic potential function into Eqs. (2.10) and (2.11), results in a new screening space charge distribution function, depicted by the red curve in Figure B.1(a). It is seen from Figure B.1(a) that the two screening space charge functions depicted deviate substantially. This deviation is an indication that the initial screening space charge distribution function, suggested by Eq. (B.1), is not a good approximation to the actual self-consistent solution of Eqs. (2.3) and (2.9). The steepness of the resultant red curve in Figure B.1(a) suggests that improved convergence might be

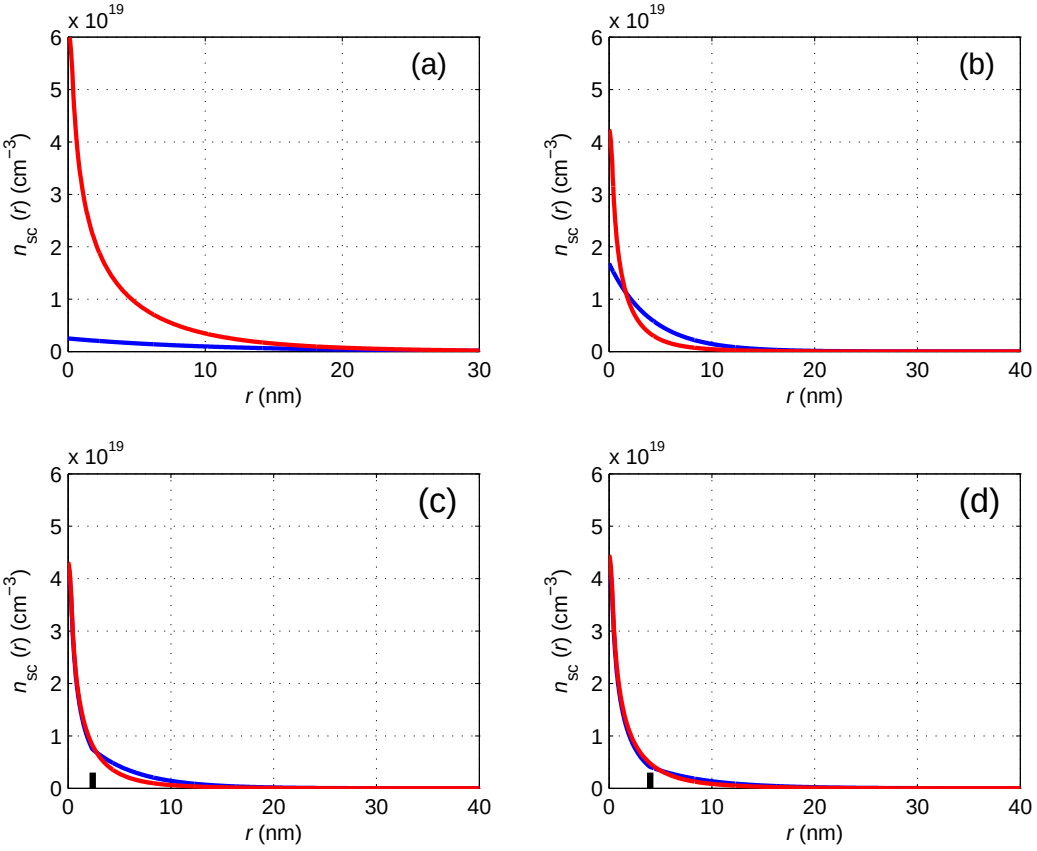

Figure B.1: An iterative construction of the screening space charge surrounding a threading dislocation line within n-type InN.

achieved by choosing a steeper exponential function than the initial guess for $n_{\mathrm{sc}}(r)$.

In Figure B.1(b), the same procedure as that used in obtaining Figure B.1(a) has been followed, however, this time, the value of λ has been selected to be 4 nm, instead of the Debye length. Note that once the value of λ is changed, the value for n_0 should also change accordingly, in order to maintain charge neutrality, i.e., equality of the negative charge subtended by the newly suggested screening space charge distribution function with the fixed positive charge in the dislocation core charge cylinder.

The next suggested approximation to the actual screening space charge distribution function is depicted with the blue curve in Figure B.1(c). For $0 \leq r < r_{\mathrm{trunc}}$, this suggested approximation is identical to the red curve in Figure B.1(b). For $r_{\mathrm{trunc}} \leq r < R_{\mathrm{sc}}$, this suggested approximation is simply an exponential function, $A \exp(-r/\lambda')$. The truncation radius, r_{trunc}, is indicated with the black line on the horizontal axis in Figure B.1(c). The two variables, A and λ', can be uniquely determined by the requirements that: (1) $n_{\mathrm{sc}}(r)$ should remain continuous at r_{trunc}, and (2) the total negative charge subtended by the newly suggested approximation to $n_{\mathrm{sc}}(r)$, should be equal to the fixed positive charge in the dislocation core charge cylinder.

In Figure B.1(d), the same procedure of replacing an exponential tail

to the red curve, obtained from the previous iteration, has been followed. The radius at which the exponential function is replaced has once again been indicated by the black line on the horizontal axis. It is observed that sufficient convergence has been reached in Figure B.1(d), i.e., a self-consistent solution to Eqs. (2.3) and (2.9) has been obtained.